

NOZZLE DESIGN AND EXPERIMENTAL EVALUATION TO MITIGATE  
LIQUID LOADING IN GAS WELLS

by  
Jagmit Singh

**© Copyright by Jagmit Singh, 2018**

All Rights Reserved

A thesis submitted to the Faculty and the Board of Trustees of the Colorado School of Mines in partial fulfillment of the requirements for the degree of Master of Science (Petroleum Engineering).

Golden, Colorado  
Date \_\_\_\_\_

Signed: \_\_\_\_\_  
Jagmit Singh

Signed: \_\_\_\_\_  
Dr. Luis E. Zerpa  
Thesis Advisor

Golden, Colorado  
Date \_\_\_\_\_

Signed: \_\_\_\_\_  
Dr. Erdal Ozkan  
Professor and Head  
Department of Petroleum Engineering

## ABSTRACT

This study consists of an experimental investigation of nozzle geometry effect on critical/subcritical flow transitions with applications on liquid loading mitigation in gas wells. Experiments were conducted in a facility with 1.5 in. ID PVC pipelines and a 30 ft long vertical section, which mimics two-phase flow (air and water) in gas wells. In total, 27 different nozzle geometries were tested, which were divided into two groups – conical and parabolic nozzles. The nozzle geometries tested were 3D printed and had a throat size of 0.25 in.

The experimental investigation was divided into three phases. The first phase consisted of a series of tests using 27 nozzle geometries in a single-phase (air) horizontal flow facility, with the purpose of determining the most optimum nozzle geometries groups based on measured key performance indicators. Phase two involved testing these top performing nozzle geometries in a two-phase (air-water) horizontal flow loop. Phase three consisted of testing the same geometries as for phase two in a two-phase (air-water) vertical flow loop, determining nozzle performance in vertical flow, comparing with horizontal flow observations and determining the most optimum nozzle geometry. A nozzle geometry was considered optimum if it exhibited the highest critical pressure ratio and at the same time minimized pressure drop across the nozzle.

Experimental results from phase 1 showed that nozzle geometry does have a significant impact on nozzle performance. Nozzles from ASTAR, Deich, LJ and Moby Dick nozzle groups showed improved performance compared to other nozzle groups. An empirical model was created based on phase 1 data in order to determine the effect of surface area of convergent and divergent section of nozzle on nozzle performance. The map created can be used to predict critical pressure ratio of a nozzle geometry by matching the nozzle design to the ones that have

been tested. It was also determined that a smaller diverging angle resulted in a higher critical pressure ratio. A nozzle with an elongated throat had a higher critical pressure ratio, but at the same time it had a higher pressure drop across the nozzle. Length of the nozzle did not have as much of an impact on nozzle performance as the throat diameter and shape of nozzle converging and diverging sections immediately before and after the throat.

Phase 2 experimental results showed that critical pressure ratio decreases when two phases are flowed through the nozzle. The length of the annular churn flow pattern observed at the exit of the nozzle may have a correlation to the nozzle performance. Based on data analysis, ASTAR nozzle geometry was the most optimum nozzle. Phase 3 data was analyzed and the most optimum nozzle geometry was determined to be ASTAR nozzle 2. Comparison with phase 2 data indicated a further drop in critical pressure ratio and an increase in pressure drop due to the effect of gravitation of the fluid flow.

## TABLE OF CONTENTS

ABSTRACT.....	iii
LIST OF FIGURES .....	viii
LIST OF TABLES.....	xi
LIST OF SYMBOLS .....	xii
ACKNOWLEDGEMENTS.....	xvi
CHAPTER 1 INTRODUCTION.....	1
1.1 Motivation of Study .....	1
1.2 Objective .....	3
1.3 Structure of Thesis .....	4
CHAPTER 2 LITERATURE REVIEW.....	5
2.1 Liquid Loading of Gas Wells.....	5
2.2 Gas Well Deliquification.....	6
2.2.1 Velocity Strings .....	6
2.2.2 Foam Injection .....	7
2.2.3 Compression .....	8
2.2.4 Plunger Lift.....	8
2.2.5 Hydraulic Lift.....	9
2.2.6 Beam Pump.....	9
2.2.7 Gas Lift .....	10
2.2.8 Electrical Submersible Pump.....	10

2.2.9	Progressive Cavity Pump .....	10
2.2.10	Nozzle .....	11
2.3	Nozzle Principles.....	11
2.4	Nozzles as Artificial Lift Systems.....	15
2.5	Nozzle Geometry Designs.....	19
2.5.1	Conical Shaped Nozzle .....	20
2.5.1.1	Converging – Diverging Nozzle.....	21
2.5.1.2	Modified Converging – Diverging Nozzle .....	21
2.5.1.3	Dual Converging Nozzle .....	21
2.5.1.4	Multi Converging – Diverging Nozzle .....	21
2.5.2	Parabolic Shaped Nozzle .....	23
2.5.2.1	Rao Nozzle .....	24
2.5.2.2	Modified Rao Nozzle.....	24
2.5.2.3	Dual Bell Nozzle .....	24
2.5.2.4	Converging Convex Nozzle.....	24
2.5.2.5	Converging Concave Nozzle.....	26
2.5.2.6	Moby Dick Nozzle.....	26
2.5.2.7	ASTAR Nozzle.....	26
2.5.2.8	Deich Nozzle .....	26
2.5.2.9	LJ Nozzle.....	28
CHAPTER 3 METHODOLOGY .....		30
3.1	Nozzle Throat Size .....	30
3.2	Experimental Matrix .....	33

3.3	Nozzle geometry drawing and 3D Print.....	35
3.4	Horizontal Facility Setup .....	38
3.5	Vertical Facility Setup.....	41
3.6	Data Collection.....	44
CHAPTER 4 RESULTS AND DISCUSSIONS .....		45
4.1	Data .....	45
4.2	Data Analysis – Single-Phase Horizontal Flow .....	48
4.3	Modelling – Single Phase Horizontal Flow .....	61
4.4	Data Analysis – Two-Phase Horizontal Flow .....	68
4.5	Data Analysis – Two-Phase Vertical Flow .....	72
4.5.1	Downstream Water Flowrate Analysis .....	74
CHAPTER 5 CONCLUSIONS AND RECOMMENDATIONS.....		77
5.1	Conclusions .....	77
5.2	Future Work Recommendation .....	78
REFERENCES .....		80

## LIST OF FIGURES

Figure 2.1	Schematic of a converging-diverging nozzle showing different sections of a typical nozzle .....	11
Figure 2.2	Leviton nozzle.....	16
Figure 2.3	Mason nozzle .....	17
Figure 2.4	Arellano nozzle .....	18
Figure 2.5	Chang nozzle.....	18
Figure 2.6	Basic conical nozzle design features and variables .....	20
Figure 2.7	Converging diverging nozzle.....	22
Figure 2.8	Modified converging diverging nozzle.....	22
Figure 2.9	Dual converging Nozzle .....	22
Figure 2.10	Multi converging diverging Nozzle .....	22
Figure 2.11	Basic design and variables for a parabolic nozzle .....	23
Figure 2.12	Rao nozzle.....	25
Figure 2.13	Modified rao nozzle .....	25
Figure 2.14	Dual bell nozzle .....	25
Figure 2.15	Converging convex nozzle.....	25
Figure 2.16	Converging concave nozzle .....	27
Figure 2.17	Moby dick nozzle.....	27
Figure 2.18	ASTAR nozzle .....	27
Figure 2.19	Deich nozzle.....	27
Figure 2.20	LJ nozzle .....	28
Figure 3.1	Results of pressure drop across choke as choke size and GLRs are varied.....	31

Figure 3.2	Pressure ratio as function of choke size, compared with estimated critical pressure ratio to identify chokes sizes that would provide choked flow at different GLRs .....	32
Figure 3.3	Gas flow rate as function of choke size, for selecting choke size based on available gas flowrate .....	33
Figure 3.4	Contour profile of a modified rao nozzle created using MS Excel.....	36
Figure 3.5	Solidworks drawing of converging – diverging conical nozzle.....	36
Figure 3.6	3D printed model of a converging diverging nozzle .....	36
Figure 3.7	Burst pressure test setup to determine the integrity of the 3D printed nozzle and ensure that it can withstand the pressures applied during experiments .....	37
Figure 3.8	Single-phase horizontal flow facility schematic .....	39
Figure 3.9	Two-phase horizontal flow facility schematic .....	40
Figure 3.10	Two-phase vertical flow facility schematic .....	43
Figure 4.1	Identify critical pressure point and pressure drop across nozzle .....	46
Figure 4.2	Dividing regions of nozzle body for pressure drop analysis.....	52
Figure 4.3	Pressure drop ratio across nozzle for single-phase horizontal flow tests.....	54
Figure 4.4	Pressure drop ratio of optimal geometries .....	55
Figure 4.5	Pressure drop ratio of non – optimal geometries .....	55
Figure 4.6	Effect of varying diverging angles on nozzle performance for conical shaped nozzles.....	56
Figure 4.7	Effect of varying throat lengths on nozzle performance for conical shaped nozzles.....	57
Figure 4.8	Effect of varying diverging angles on nozzle performance for parabolic shaped nozzles.....	58
Figure 4.9	Effect of varying throat lengths on nozzle performance for parabolic shaped nozzles.....	59
Figure 4.10	Effect of nozzle length on nozzle performance .....	60
Figure 4.11	Effect of converging, throat and diverging surface area on nozzle configuration performance by applying dimensionless analysis.....	65

Figure 4.12	Pressure drop and critical pressure ratio against X to determine the optimal geometries.....	66
Figure 4.13	Effect on nozzle performance of varying diverging angle for different nozzle geometry groups.....	67
Figure 4.14	Effect on nozzle performance of varying throat length for different nozzle geometry groups.....	68
Figure 4.15	Pressure drop ratio across nozzle for two-phase horizontal flow tests .....	70
Figure 4.16	Stratified flow pattern upstream of nozzle.....	71
Figure 4.17	Annular churn flow pattern downstream of nozzle before turning back to stratified flow .....	71
Figure 4.18	Effect of length of annular churn flow pattern downstream of nozzle on nozzle performance .....	72

## LIST OF TABLES

Table 3.1	Nozzle Geometries Created to Conduct Single-Phase and Two-Phase Experiments by Varying Design Parameters .....	34
Table 4.1	Single-Phase Horizontal Flow Experimental Results .....	47
Table 4.2	Two-Phase Horizontal Flow Experimental Results .....	48
Table 4.3	Two-Phase Vertical Flow Experimental Results .....	48
Table 4.4	Ranking of Nozzle Performance Based on Critical Pressure Ratio .....	49
Table 4.5	Ranking of Nozzle Performance Based on Pressure Drop Across Nozzle .....	50
Table 4.6	Rank of Nozzles Based on Both Critical Pressure Ratio and Pressure Drop .....	51
Table 4.7	Effect of Pressure Transducers on Nozzle Performance .....	61
Table 4.8	Calculated Values of Dimensionless Number for Nozzle Tested .....	64
Table 4.9	Ranking of Nozzle Performance Based on Critical Pressure Ratio .....	69
Table 4.10	Ranking of Nozzle Performance Based on Pressure Drop Across the Nozzle .....	69
Table 4.11	Rank of Nozzle Performance Based on Both Critical Pressure Ratio and Pressure Drop .....	69
Table 4.12	Comparison of Data between Horizontal and Vertical Two Phase Flow .....	74
Table 4.13	Downstream Water Flowrate Calculation Data and Results .....	75

## LIST OF SYMBOLS

$A$	Area
$A_p$	First coefficient of equation for diverging parabolic section
$a_0$	First coefficient of equation for converging circular section
$a_1$	First coefficient of equation for converging concave circular transition section
$a_2$	First coefficient of equation for diverging concave circular transition section
$B_p$	Second coefficient of equation for diverging parabolic section
$b_0$	Second coefficient of equation for converging circular section
$b_1$	Second coefficient of equation for converging concave circular transition section
$b_2$	Second coefficient of equation for diverging concave circular transition section
$C$	Velocity
$C_d$	Discharge coefficient
$C_p$	Third coefficient of equation for diverging parabolic section
$C_1$	Velocity at point 1
$C_2$	Velocity at point 2
$c_0$	Third coefficient of equation for converging circular section
$c_1$	Third coefficient of equation for converging concave circular transition section
$c_2$	Third coefficient of equation for diverging concave circular transition section
$D_t$	Throat diameter
DPT	Differential pressure transmitter
$dA$	Change in area
$dh$	Change in enthalpy

$dQ$ .....	Change in heat transferred
$du$ .....	Change in internal energy
$dP$ .....	Change in pressure
$dC$ .....	Change in velocity
$dv$ .....	Change in volume
GLR .....	Gas Liquid Ratio
$h$ .....	Enthalpy
$h_1$ .....	Enthalpy at point 1
$h_2$ .....	Enthalpy at point 2
$K$ .....	Constant 1
$L_c$ .....	Length of converging section
$L_d$ .....	Length of diverging section
$L_t$ .....	Throat length
$M$ .....	Mach number
$m_1$ .....	Multiplier for converging throat longitudinal radius
$m_2$ .....	Multiplier for diverging throat longitudinal radius
$n$ .....	Specific heat ratio
$P$ .....	Pressure
PT .....	Pressure transducer
PI .....	Productivity Index
$R$ .....	Produced gas liquid ratio
$R_1$ .....	Throat longitudinal radius
$S_{con}$ .....	Surface area of convergent section

$S_{cir,c}$	.....	Surface area of converging circular section
$S_{ct,c}$	.....	Surface area of converging concave circular transition section
$S_{lin,c}$	.....	Surface area of converging linear section
$S_{div}$	.....	Surface area of divergent section
$S_{ct,d}$	.....	Surface area of diverging concave circular transition section
$S_{lin,d}$	.....	Surface area of diverging linear section
$S_{p,d}$	.....	Surface area of diverging parabolic section
$S_{th}$	.....	Surface area of throat section
TT	.....	Temperature transducer
X	.....	Dimensionless number
u	.....	Internal energy
v	.....	Volume
$v_s$	.....	Speed of sound
$\alpha$	.....	Diverging angle
$\alpha_1$	.....	Converging angle at first coordinate of converging section
$\alpha_2$	.....	Converging angle at last coordinate of converging section
$\beta$	.....	Converging angle
$\beta_1$	.....	Diverging angle at last coordinate of throat
$\beta_2$	.....	Diverging angle at last coordinate of diverging concave circular transition section
$\delta_1$	.....	Kronecker delta for converging linear section
$\delta_2$	.....	Kronecker delta for converging circular section
$\delta_3$	.....	Kronecker delta for converging concave circular transition section
$\delta_4$	.....	Kronecker delta for throat section

$\delta_5$  ..... Kronecker delta for diverging concave circular transition section  
 $\delta_6$  ..... Kronecker delta for diverging parabolic section  
 $\delta_7$  ..... Kronecker delta for diverging linear section  
 $\epsilon_c$  ..... Orifice downstream to upstream ratio at critical conditions  
 $\rho$  ..... Density  
 $d\rho$  ..... Change in density

## ACKNOWLEDGEMENTS

First, I would like to thank my advisor Dr. Luis Zerpa, for his support throughout this project. I really appreciate his willingness to take over the role as the principle advisor for this project after some unexpected events took place. His valuable contribution and suggestions regarding the project were the reason why I was able to produce the best results possible and complete the project of time. He would go out of his way to guide me to proper resources to help me deliver my best.

I would also like to thank Chevron, not only for their financial support for me to successfully complete this project, but also for their continuous technical guidance. In particular, I would like to thank Jose Gamboa and Ben Partington. I appreciate the time they took out every month to have a meeting and provide valuable input on the data that obtained. I would also like to thank Dr. Mansur Ermila for being the committee chair and providing valuable input to improve the thesis.

I am also very grateful to all the colleagues who worked along with me on this project at different times - Daniel Croce for his guidance throughout this project and his help purchasing and installing the equipment; Hugo Cordova for his help conducting the experiments and also setting up the facility; Max Taktarov and Matthew Pinello for their help in setting up the experimental facility; Charles Baxter and Lucas Morse for their help with creating the SolidWorks drawings.

Finally, I would like to thank my family – dad (Manjit Singh), mom (Arvinder), brother (Baljit) and sister (Jessie). They were a constant pillar of support during my time at CSM and provided me with the encouragement to do my best at anything that I attempted.

## CHAPTER 1

### INTRODUCTION

Liquid loading is a major challenge that is faced during production from gas wells. Liquid loading is defined as the accumulation of liquids at the bottom of the well, when the dominant gas phase is not able to lift all produced liquids to the surface, mainly due to gravity effects. Artificial lift techniques can be implemented to successfully deliquify gas wells, i.e., carry liquids out of the well. But these techniques can be expensive to implement and run as they may have high OPEX and CAPEX associated with them. Hence, there is a need for a more economical artificial lift system to deliquify wells efficiently. A nozzle attached on a tubing to increase the gas velocity can perform as an economical artificial lift system and is studied in this research. In particular, the design parameters of nozzle geometry are modified in order to determine the optimum nozzle geometry that can efficiently deliquify a well. An optimum nozzle geometry should maximize the critical pressure ratio and minimize the inlet-outlet pressure drop across the nozzle. By achieving these key performance indicators, a loaded well can be efficiently and optimally deliquified.

#### **1.1 Motivation of Study**

A well is considered ‘loaded’ when gas velocity falls below the critical gas velocity, which is the minimum gas velocity required to remove liquids from the well. When this occurs, liquid starts accumulating in the tubing or casing or both and creates a buildup, which causes a sharp decline in production rate. This lower production results in a lower revenue stream for the company. Some of the reasons that can result in the onset of liquid loading include a decline in

reservoir pressure over a period of time, productivity index (PI) degradation due to reservoir, completion or operational issues, holes in tubing or an unexpected increase in wellhead pressure.

In conventional wells, Turner's model can be implemented to predict the onset of liquid loading. Since the timeframe of when liquid loading will occur is known, artificial lift methods can be implemented in advance to minimize this issue (Turner 1969). However, for unconventional horizontal wells, there is no accurate model to predict the onset of liquid loading since Turner's model does not account for the change in inclination angle of the well. Therefore, artificial lift methods, at times, are implemented only after liquid loading has started to occur.

Currently, different artificial lift techniques are being implemented in order to deliquesfy gas wells. Some of these conventional techniques include gas lift, plunger lift, foam injection, wellhead compression, reducing tubing diameter and direct pumping (sucker rod pumps, electrical submersible pumps, progressive cavity pumps and hydraulic pumps). These methods, however, have their drawbacks that include size of surface or sub-surface equipment required, amount of gas required which is not always available, workover risks associated with each method. This decreases their cost efficiency due to high OPEX and CAPEX associated with them. (Lea and Nickens 2004)

Nozzles as an artificial lift system can help solve problems of conventional artificial lift methods as it is a very cost efficient artificial lift method, mainly due to its ease of installation and low workover requirements. When a nozzle is installed in a well it basically acts as a choke and behaves according to the Venturi principle. However, unlike an orifice choke, there is no sudden reduction or expansion in the size of the flow area. Instead, there is a gradual tapering down of the cross-sectional area until the throat and then there is a gradual tapering up to the tubing string size. As fluids move through the converging section of the nozzle and then into the

throat, they accelerate because of a decrease in flow area of nozzle and this causes the fluids to travel the tubing string at a faster velocity.

Due to limited studies conducted on the performance of nozzles in multiphase flow systems and their use as an artificial lift method, nozzles are not yet widely used in field applications. Most of the studies performed either consider just one fixed nozzle geometry (Levitan et al. 2000) or use a nozzle that atomizes the fluid flowing through it, which results in high pressure drop due to very high velocities of gas and liquid (Mason et al. 2007). This may be an optimum design, but no comparison is made to a nozzle that does not atomize the fluid flowing through it but is still effective to mobilize liquids to the surface. It is believed that nozzle geometries have varying effects on the flow through the nozzle, resulting in varying pressure drops. Currently in the industry, choke equations are used to size the nozzle throat section. However, this is not accurate since these equations do not consider the diffuser section of a nozzle, which has significant impact on nozzle performance. The choke design equations also assume that the flow between gas and liquid phase is homogenous, which is not the case.

## **1.2 Objective**

The primary objective of this experimental study is to evaluate the effect of nozzle geometry on key performance measures during single and two-phase flow. To achieve this, different nozzle configurations will be experimentally tested as they are installed on small-scale horizontal and vertical flow loops. These loops will mimic liquid and gas flow in horizontal and vertical wells respectively. Several variables, such as pressures, temperatures, gas and liquid flowrates will be recorded along the pipeline system as the fluid moves through the nozzle. This data will be analyzed to determine the optimal nozzle configuration to maximize critical pressure ratio and at the same time minimize pressure drop across the nozzle.

### **1.3 Structure of Thesis**

This thesis is divided into five chapters. Chapter 2 discusses the literature review performed during this project which includes the basics of liquid loading, artificial lift methods that are implemented in order to deliquefy a loaded well, current status in the industry of using nozzles as an artificial lift method and different shapes of nozzles that were used as basis to design different nozzle geometries. Chapter 3 discusses the methodology that was followed in order to achieve the objective of this project, which includes determining the experimental matrix, designing and 3D printing the nozzle and constructing the horizontal and vertical facility setups. Chapter 4 shows the data that was obtained after performing the experiments and the data analysis that was performed in order to determine the optimum nozzle geometry. Chapter 5 provides the conclusions drawn from this research study and discusses future research that can be performed on related topics.

## CHAPTER 2

### LITERATURE REVIEW

This chapter will provide the background and knowledge regarding liquid loading in gas wells, different artificial lift methods implemented to deliquify gas wells, basic principles of flow through a nozzle, and types nozzle geometries considered in this experimental study.

#### **2.1 Liquid Loading of Gas Wells**

About a third of the producing wells in the US are gas wells (EIA 2018). All of these wells produce liquids in one or more forms – condensate, connate water, evaporated water and stimulation flowback fluid. At early stages of production, gas velocity is high enough to carry the liquids to the surface. But as these wells age, the bottom hole pressure declines, which results in a decline in gas velocity. A decline in gas velocity below the point of critical gas velocity can lead to erratic, sluggish flow that results in liquid loading. When the gas velocity is too low, pressure gradient in the tubing increases due to the accumulation of liquids at the bottom of the well. This increase in back pressure against the reservoir lowers the production further and exacerbates the issue of liquid loading.

Liquid loading is experienced by all gas wells that produce liquids at some point in their producing life. Even wells that have high gas-liquid ratios and small liquid rates can experience this phenomenon if the gas velocity is less than the critical gas velocity. In wells where no packer is installed and tubing is not cemented in, the onset of liquid loading can be identified by examining the change in tubing and casing pressures. When liquid loading occurs, the surface tubing pressure lowers and the surface casing pressure increases. Surface tubing pressure lowers as a result of increased back pressure on the formation due to accumulation of liquids. And

surface casing pressure increases because the gas that percolates into the tubing-casing annulus is exposed to higher formation pressure causing an increase in the surface pressure. Liquid loading can also be identified by examining the liquid production. If the production of liquid drops dramatically it means that the liquid is not being produced along with gas and is building up downhole. Also, comparing the current production rate to the expected production rate can provide a sign that liquid loading is occurring. (Lea and Nickens 2004)

Once these signs are noticed, it is important to take some actions to restore the well back to its optimum production cycle. If nothing is done the production can decline to a point where the well stops producing due to liquid buildup.

## **2.2 Gas Well Deliquification**

Deliquification of a well is of paramount importance once liquid loading occurs. This entails removing water or condensate buildup from producing wells. Artificial lift techniques can be used in order to deliquefy a well. Selection of an optimal artificial lift depends on many factors that include producing characteristics, fluid properties, hole characteristics, reservoir characteristics, surface facility, location, available of power sources, operation challenges and the CAPEX and OPEX associated with the artificial lift method. The following artificial lift techniques are widely used in the industry:

### **2.2.1 Velocity Strings**

Based on the Inflow Performance Relationship (IPR) and Outflow Performance Relationship (OPR), an optimum tubing size can be chosen that will help minimize the effect of liquid loading. A smaller size tubing or velocity string can increase the gas velocity and help carry the liquids to the surface. This method can be implemented in deviated or vertical wells, onshore or offshore. In certain cases, it can also be carried out under pressure, i.e., there is no

need to kill the well in order to install the string (Oudemans 2007). But it is not an effective long-term solution. By installing a smaller size string, the gas velocity increases in the well. This increase in gas velocity will result in a higher frictional pressure drop and lower production rates. Therefore, eventually another method would have to be used in order to keep the well flowing. Another challenge occurs while designing the string. It is very important that the calculations performed in order to create the required behavior are accurate. Else, if the pressure drop is overestimated the tubing size will be too big; this would result in higher production rates, but only for a short period of time because liquid loading would occur again. And if the pressure drop is underestimated, the tubing size would be too small; this would result in an excessive drop in production rates.

### **2.2.2 Foam Injection**

Foaming agent is injected into the well to lower the density and surface tension of the liquid. The liquid is held in a bubble film and exposed to more surface area, which results in less gas-slippage. As the effective density of liquid column is reduced, the tubing pressure gradient reduces as well. This mixture is then easily carried to surface by gas as the critical gas velocity required is lowered (Lea and Nickens 2004). For low rate gas wells, dropping soap sticks is a cost effective solution, as no downhole equipment is generally required. Using foams as a deliquification method can result in liquid emulsion problems due to foam carryover. For a foaming agent to work successfully, it needs to be agitated so gas can mix with the liquid and lighten it. But if condensates are present in the well, due to their non polar nature, they do not mix as well with foams. Therefore, a high amount of special foaming surfactants or additional equipment is required in order to generate sufficient agitation. This may lower the cost efficiency of this method. (King 2005)

### **2.2.3 Compression**

Compression technique involves lowering the wellhead tubing pressure by using a compressor. This decrease in wellhead pressure will result in an increase in gas velocity due to the higher pressure differential between surface and reservoir and help move the liquids to the surface. This technique in some cases can be the lowest risk and most economical option to implement. For example, if there are restrictions present downhole in the tubing, compression is a better option as downhole equipment for artificial lift techniques might be more expensive to install past the restrictions. Also, other techniques may lower the flow area in the tubing due to the presence of equipment that can result in excessive pressure drops. The issue with compression however is that it cannot be applied effectively since the reservoir itself is affected. There may be problems such as fines migration and other erosional issues that may result in requiring expensive completions. Also, in order to lower the wellhead pressure, large-scale expensive surface facilities such as compressor are required which lowers the cost effectiveness of this technique (Lea and Nickens 2004).

### **2.2.4 Plunger Lift**

Plunger lift is a type of an intermittent artificial lift system that involves using a free moving piston to lift the accumulated liquids to the surface using energy of the reservoir. This system is small and easy to install. It does not require any external power source or workover rig to install. But it does require set up of surface equipment such as lubricators, catcher assembly and springs and also requires modifications to the wellhead, which adds to the initial installation costs. This method is also challenging to implement in offshore wells. The constant surges of gas and liquid to the surface facilities may erode surface facilities if they are not designed properly.

Also once the reservoir pressure is too low, it cannot support the movement of the plunger and another lift system would be required (Joseph et al. 2013).

### **2.2.5 Hydraulic Lift**

Hydraulic pumps are installed in the tubing downhole and are powered by applying pressure from the surface using a ‘power fluid’ that flows from the surface to the pump. These pumps can be jet pumps, where fluid is directed into the nozzle of the pump, or they can be piston pumps. These pumps are capable of increasing the pressure at the point where fluid enters the pump by using the power fluid. This increased pressure difference between this point and the surface results in the fluid travelling up the tubing. These pumps work well in changing production rates and are able to produce at greater depths compared to other pump systems. But they require high initial costs due to a need of high pressure surface equipment. The power fluid must be conditioned and removed of sand and other particles to avoid damage to the pump (Lea and Nickens 2004), which increases power oil costs and maintenance costs.

### **2.2.6 Beam Pump**

Beam pumps are a very common system used to produce liquids from a gas well. These pumps are based on opening/closing of valves in order to let the liquids into the pump and then out. Their ease of use, availability and understanding of the principle have made them a popular choice. But they require a huge initial investment relative to other methods. A major issue with beam pumps is that they are prone to experience ‘gas locking’, which is when the barrel is completely filled with free gas and the standing valve cannot open on the upstroke to allow the flow of liquids since the pressure in the barrel is not low enough. They are also depth and deviation limited, as they are dependent on the capability of the rod. They have limited tolerance sand production that well and are limited to only onshore applications. (Lea and Nickens 2004)

### **2.2.7 Gas Lift**

Gas lift involves injecting a stream of gas into the production tubing through a valve that will result in lowering the density of the liquid present in the tubing. This will help the gas carry the liquid to the surface. Gas lift can be employed in situations such as wells with high GLR and highly deviated wells. Production of solids does not affect this artificial lift system and it can be easily altered to adapt to changes in reservoir conditions. However, implementation of this technique is very dependent on the availability of a natural gas source. Initial costs can also be high if compressors are required. Continuous gas lift cannot be implemented for a long time, as problems arise when the BHP lowers significantly (Lea and Nickens 2004). Also, gas lift mandrels need to be installed to position gas lift valves, for which the tubing has to be pulled.

### **2.2.8 Electrical Submersible Pump**

Electrical Submersible Pump is a multistage centrifugal pump that is powered by a downhole motor. It can lift high volumes, has a small footprint and can be used in offshore applications. But, high volume of gas can cause gas interference and severely damage to the pump, reducing its efficiency to lift liquids out of the well. They are also the most expensive form of artificial lift method as they are associated with high installation and operational costs (Lea and Nickens 2004). They also require a reliable source of electricity and cable, which are prone to failures due to high temperature and corrosion and also are depth limited.

### **2.2.9 Progressive Cavity Pump**

A Progressive Cavity Pump involves the use of a rotor and a stator to move the fluids out of the well. These pumps are very efficient and are moderately expensive. They are simple to install and operate and can tolerate large volume of solids, liquids and viscous fluids. However, there are some drawbacks too, for example the elastomers in the stator may swell and the rotor

may cause damage to the tubing. Also they are generally only used for wells with low rates and at shallow depths (Lea and Nickens 2004).

### 2.2.10 Nozzle

The following sections discuss the basic principles of flow through a nozzle, its operation and geometry, its advantages as an artificial lift method and current status of implementing nozzle as artificial lift system in the industry.

## 2.3 Nozzle Principles

Nozzles have three different sections – converging section, throat and diverging section, as shown in Figure 2.1. The point where the diameter of the nozzle is the smallest is called the throat. Throat can either be a single point or it can be elongated. Section upstream of the throat is the converging section, and section downstream of throat is the diverging section. The area of the converging section decreases as the nozzle profile goes from pipe to the beginning of throat. The area of diverging section increases as the nozzle profile goes from the end of the throat to the pipe.

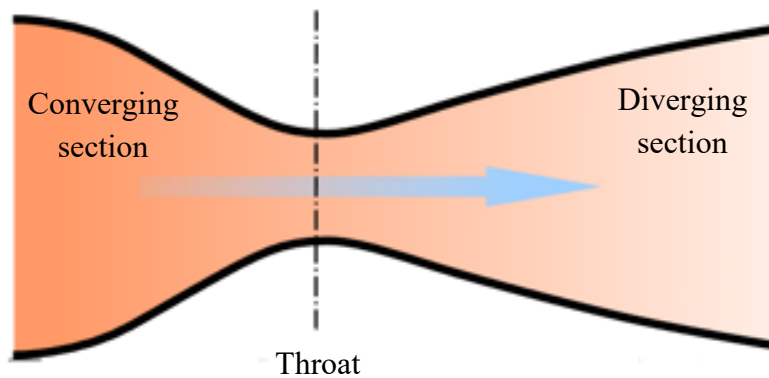


Figure 2.1 Schematic of a converging-diverging nozzle showing different sections of a typical nozzle (Clarke and Carswell 2007)

Fluid flow behavior through nozzles depends on the type of fluid flowing through the nozzle. The dimensionless Mach number, which is the ratio of velocity at which the fluid is

flowing to velocity of sound in the surrounding medium, can be calculated in order to determine if the flow is compressible ( $M > 0.2$ ) or incompressible ( $M < 0.2$ ). If the fluid is incompressible such as liquids, where the density is constant for fluid flow at every point, velocity of the fluid flowing through the nozzle is inversely proportional to the surface area of the nozzle. As area decreases in the converging section, the static pressure is converted to kinetic energy by acceleration of flow. When fluid flows through the diverging section, the area increases which converts kinetic energy to static energy by slowing the fluid velocity (Levitan et al. 2000). So, pressure behaves in an inverse relation to velocity, i.e., when velocity increases the pressure drops and vice-versa.

If the fluid is compressible such as air, where the density changes from point to point, thermodynamic changes during the flow cause the fluid to behave differently compared to incompressible flow. As the fluid enters the nozzle, the velocity increases until the throat of the nozzle is reached. At this point the flow is subsonic, i.e.,  $M < 1$ . Once fluid flows through the throat, given sufficient upstream pressure and flowrate conditions, velocity of fluid becomes equal to the velocity of sound and reaches sonic conditions, i.e.,  $M = 1$ . And as the fluid leaves the throat and enters the diverging section, the velocity increases, unlike incompressible flow, and becomes greater than the speed of sound to reach supersonic flow, i.e.,  $M > 1$ . This occurs because when air is flowing through the diverging section of the nozzle, there is an increase in kinetic energy at the expense of an enthalpy drop due to gas expansion. This can be mathematically expressed as:

$$h_1 - h_2 = \frac{C_2^2}{2} - \frac{C_1^2}{2} \quad (2.1)$$

Rearranging this equation,

$$h_1 + \frac{C_1^2}{2} = \frac{C_2^2}{2} + h_2 \quad (2.2)$$

Since the addition of enthalpy and kinetic energy throughout the flow is constant, the above equation can be rewritten as,

$$h + \frac{C^2}{2} = K \quad (2.3)$$

Differentiating the above equation w.r.t. velocity,

$$dh = -CdC \quad (2.4)$$

Enthalpy is defined as,

$$h = u + Pv \quad (2.5)$$

Differentiating w.r.t. to internal energy and rearranging the equation,

$$dh = du + Pdv + vdP \quad (2.6)$$

Since there is no heat added to the system or none leaving the system, heat transferred is

0. Then,

$$dQ = du + Pdv = 0 \quad (2.7)$$

$$dh = vdP \quad (2.8)$$

Or,

$$-CdC = vdP \quad (2.9)$$

Dividing this equation (2.9) with  $C^2$  and replacing volume by inverse of molar density,

$$\frac{dC}{C} = -\frac{dP}{\rho C^2} \quad (2.10)$$

The equation of continuity in its differential form is given as,

$$\frac{dC}{C} + \frac{d\rho}{\rho} + \frac{dA}{A} = 0 \quad (2.11)$$

Upon substitution,

$$-\frac{dP}{\rho C^2} + \frac{d\rho}{\rho} + \frac{dA}{A} = 0 \quad (2.12)$$

$$\frac{dA}{A} = \frac{dP}{\rho C^2} \left[ 1 - \frac{d\rho C^2}{dP} \right] \quad (2.13)$$

From Newton-Laplace equation, speed of sound can be defined as

$$\sqrt{\frac{dP}{d\rho}} = v_s \quad (2.14)$$

Upon substitution,

$$\frac{dA}{A} = \frac{dP}{\rho C^2} \left[ 1 - \frac{C^2}{v_s^2} \right] \quad (2.15)$$

Mach number,

$$M = \frac{C}{v_s} \quad (2.16)$$

Therefore,

$$\frac{dP}{dA} = \frac{\rho C^2}{A(1 - M^2)} \quad (2.17)$$

Under supersonic flow conditions ( $M > 1$ ), density, velocity and area cannot be negative.

Therefore,

$$\frac{dP}{dA} = (\text{negative}) \quad (2.18)$$

And,

$$dP \propto -dA \quad (2.19)$$

As velocity increases between two points, pressure decreases. So  $dP$  would always be a negative value. For  $dP$  to be negative,  $dA$  would have to be positive. This would entail that area

at point 2 would have to be greater than area at point 1, which is the case in the divergent section of the nozzle.

The goal of using a nozzle is to accelerate the flow through it such that critical or sonic condition is achieved at its throat, i.e., the flow is choked. This happens as the pressure differential downstream and upstream the nozzle increases. At a certain differential pressure, the flowrate through the nozzle for that particular throat size reaches a maximum. Any further increase in pressure differential does not result in an increase in flowrate. Beyond the point where flowrate stops increasing, the flow is said to be choked. The flow is choked when the velocity of the fluid flowing through the nozzle reaches a Mach number of 1 at the throat. Once this happens, any perturbation that occurs downstream to the throat of the nozzle would not affect the inflow from the reservoir. It is very beneficial to achieve choked flow, as any modification that maybe required in the downstream facilities or any other pressure or flow disturbances that may occur downstream from the throat would not affect the flow upstream the throat. This will ensure consistent production from the well regardless of any situation downstream the throat.

In the petroleum industry, the application of nozzle as an artificial lift system to deliquescent gas wells has not been studied extensively yet. Because of this there is limited research on the performance of nozzles in multiphase flow systems and their use as an artificial lift method. The next section goes into details of current research regarding nozzle flow and nozzle design and how they have been implemented in field applications.

## **2.4 Nozzles as Artificial Lift Systems**

One of the first studies that can be found in the literature regarding the use of nozzles as an artificial lift method is by Levitan et al. In 2000, they patented a ‘method and apparatus for

withdrawal of liquid phase from wellbores' which works by installing a device within the well which included a mandrel with a nozzle installed inside (Figure 2.2) and a sealing assembly above the nozzle (Levitan et al. 2000). The design of the nozzle used in this patent is based on a de Laval nozzle. Nozzle design is a critical parameter to have optimum flow by reducing the pressure drop through the nozzle. In this case however, the de Laval nozzle design may not be the optimum configuration for critical flow.

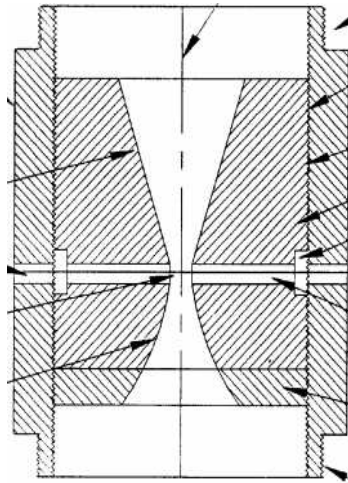


Figure 2.2 Levitan nozzle

Mason et al. in 2007 patented a 'Venturi Siphon Atomization Liquid Apparatus and Method' that can be installed in the casing or tubing. This apparatus consists of a sealing element on top of which an axially installed converging-diverging nozzle can be placed (Figure 2.3). The goal of this apparatus is to atomize the liquid droplets as they move through the nozzle (Mason et al. 2007). Atomization results in a decrease in liquid droplet size and dramatically decreases the required velocity to lift the liquid from the bottom of the well to the surface (Turner et al. 1969). This is a short-lived effect as the liquid droplets that exit the nozzle eventually coalesce to form a liquid film. It is uncertain how far can the liquid droplets be carried as mist. Atomization

also increases the velocity of the liquid because of smaller throat size and will result in very high-pressure losses. This may reduce the efficiency of this system as an artificial lift method.

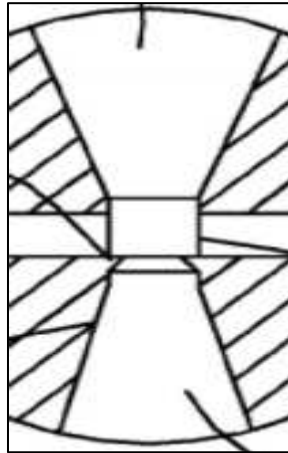


Figure 2.3 Mason nozzle

In 2015, Arellano and Ermel patented an artificial lift system to deliquify gas wells, which embodied a nozzle that could be attached to the production tubing (Arellano and Ermel 2015). This nozzle has both parabolic and conical contours and no elongated throat, as shown in Figure 2.4. Application of this nozzle was tested in an experimental study performed at University of Tulsa in association with Chevron in ‘Downhole Venturi Nozzles and Foam Application: A Novel Artificial Lift Method’ (Nair et al. 2015). In order to determine the optimum throat size of the nozzle, equations used to design chokes were used. However, this is not believed to be correct because fluid flow through a choke and a nozzle behave in different ways. Equations to represent flow of fluids through a choke do not account for the diffuser section of the nozzle. This results in inaccurate critical pressure ratio calculation. Another drawback of using the choke design equations is that these equations are based on a fundamental assumption that the flow is homogenous, i.e., there is no slip between gas and liquid phase and they are flowing at the same velocity. But this assumption is not valid since liquid and gas phase

flow at different velocities relative to each other depending on the flow pattern. The flow pattern at the entrance of the nozzle is different from the flow pattern at the exit of the nozzle, therefore the slip condition should be accounted for.

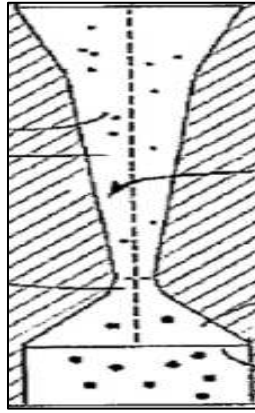


Figure 2.4 Arellano nozzle

In 2017, Chang and Bai published a paper which provides a method to deliquesfy gas wells using a supersonic nozzle. In this study, a converging-diverging nozzle (Figure 2.5) was designed which atomizes the liquid that is flowing through the nozzle. Both converging and diverging sections of this nozzle have a parabolic profile (Chang and Bai 2017). Atomization is the principle applied here for deliquification, which as mentioned above is not an efficient technique. The Mach number increases along the profile as the fluid flows through the nozzle. This increase in velocity results in a high pressure drop across the profile.

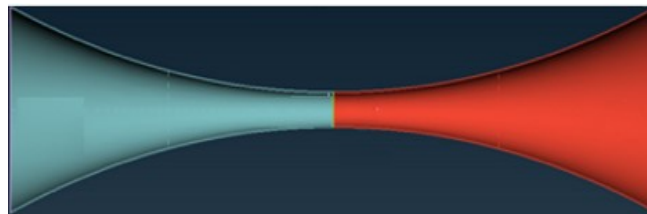


Figure 2.5 Chang nozzle

As discussed in a previous section, current artificial lift techniques have their drawbacks.

Nozzle as an artificial lift system has the following advantages over other methods:

- It is the most inexpensive form of artificial lift technique. It can be deployed simply by slickline, which means there is no need for a workover rig to pull the tubing.
- Nozzles could easily be combined with other artificial lift methods such as foams in order to increase its efficiency.
- No need for gas injection, any auxiliary equipment or surface equipment (Chang and Bai 2017).
- There are no moving parts in the apparatus. Therefore, chances of fishing or other workover remedial operations related to nozzle artificial lift method are very low.
- In offshore applications, a nozzle can be installed below the sub-surface safety valve, which improves its applicability.

There is a limited amount of research that has been performed to study the behavior of these devices in field applications and under multiphase flow conditions. As a consequence, there is an urgent need to evaluate the performance of different nozzle geometries under multiphase flow conditions and optimize the profile design to deliquefy gas wells.

## **2.5 Nozzle Geometry Designs**

Review of research in industries other than oil and gas regarding flow through nozzle was performed. These studies employed different nozzle designs, but not all of them justify the reasoning behind the selected shape and geometry. The question of which geometry would work best to deliquefy gas wells is a major research question that this study will address. In this section, different nozzle designs and the factors affecting nozzle performance will be discussed.

The basic shapes of the nozzles can be characterized into two - conical shape and parabolic shape.

### 2.5.1 Conical Shaped Nozzle

A conical nozzle, or a converging-diverging nozzle, has a downward tapering linear inlet area which reduces along the profile in cross-sectional area until the throat diameter has been reached, and then has an upward tapering linear outlet area where the cross-sectional area increases along with the profile, as shown in Figure 2.6. The angle at which the inlet tapers is called converging half-angle ( $\beta$ ). The angle at which the outlet tapers is called the diverging half-angle ( $\alpha$ ). The diameter of the smallest point in the nozzle is called the throat diameter ( $D_t$ ). The length of the nozzle is nozzle length. The throat longitudinal radius is represented as  $R_1$ .

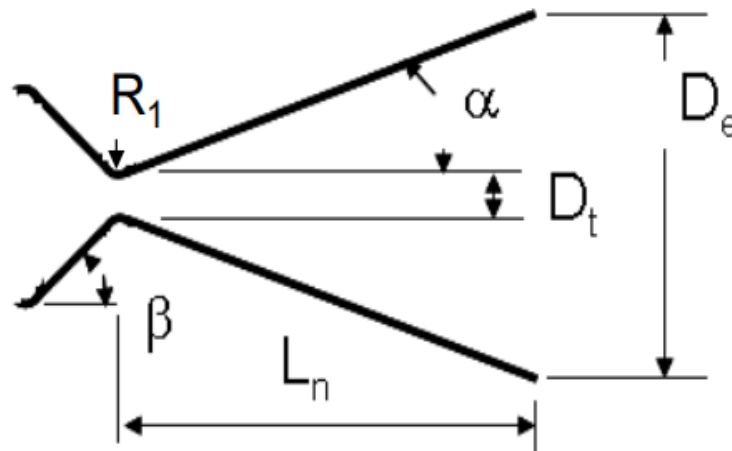


Figure 2.6 Basic conical nozzle design features and variables (Sutton and Biblarz 2001)

The cone divergence half-angle should not exceed 15 degrees, to avoid nozzle internal flow losses (Östlund 2002). According to Barber, the value of cone divergence half angle should be between 2 - 12 degrees (Barber and Schultheiss 1967). Limited studies provide a definitive value or range of the converging half-angle, but generally it is about 45 degrees. Varying the converging angle possibly does not have as much effect as the diverging half angle, because the

flow is still sub-sonic in the converging region of the nozzle, but varying the shape of the converging section may have impact on the pressure drop across the nozzle.

There are four different conical nozzle designs that were considered to conduct experiments with. Designs for conical shape-based nozzles include the following:

#### **2.5.1.1 Converging – Diverging Nozzle**

This is a basic de Laval nozzle without an elongated throat that is used in many applications such as steam turbines and rocket engines (Figure 2.7).

#### **2.5.1.2 Modified Converging – Diverging Nozzle**

The design of this nozzle is very similar to the design of the nozzle mentioned above except this has an elongated throat length (Figure 2.8). In the technical report ‘Acceleration of liquids in two phase nozzles’ by NASA, it was determined that throat length had an impact on the performance of the nozzle (Elliot and Weinber 1968). In order to determine the effect of throat length, this profile will be tested in this project.

#### **2.5.1.3 Dual Converging Nozzle**

Design for a dual converging nozzle (Figure 2.9) was obtained from a patent of a liquid gas injector in the industry of jet technology (Popov et al. 2002). It has two subsequent converging sections with decreasing converging angle.

#### **2.5.1.4 Multi Converging – Diverging Nozzle**

Two different designs were obtained from “Numerical Investigation of Two Phase Nozzle Flow” by Rahman et al. They performed CFD simulations to study the effect of two phase atomization performance. It was determined that a higher number of converging-diverging sections (Figure 2.10), resulted in higher turbulence in the nozzle and smaller droplet diameters (Rahman et al. 2014).

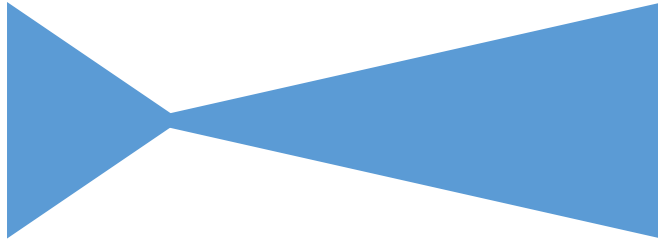


Figure 2.7 Converging diverging nozzle

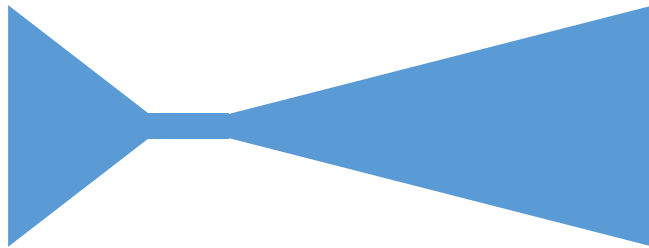


Figure 2.8 Modified converging diverging nozzle

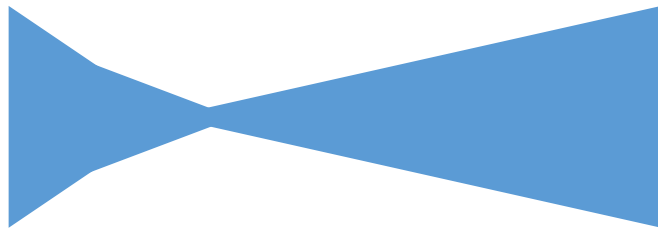


Figure 2.9 Dual converging Nozzle

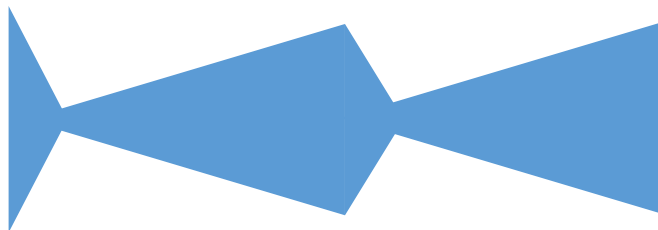


Figure 2.10 Multi converging diverging Nozzle

## 2.5.2 Parabolic Shaped Nozzle

A bell or Rao nozzle, has a circular converging section and a parabolic diverging section. The point from which the parabolic diverging section begins is called nozzle angle ( $\theta_n$ ). The angle created at the end of the nozzle is termed as nozzle exit ( $\theta_e$ ). Equations to design this nozzle are similar to the ones that are used to design nozzles for rockets. The radius of the circular converging section is 1.5 times the throat radius. This region continues until the throat is reached. Once the profile of the throat ends, another circle of radius 0.382 times the throat radius is designed. The slope of parabolic curve is tangent to the inflection point ( $\theta_n$ ), where the divergent curve and the parabolic curve intersect (Kulhanek 2012). Then at a certain point, a parabola of bell shape is created which constitutes majority of the diverging area. Based on the general equation of a parabola profile of nozzle as shown in Figure 2.11 was created.

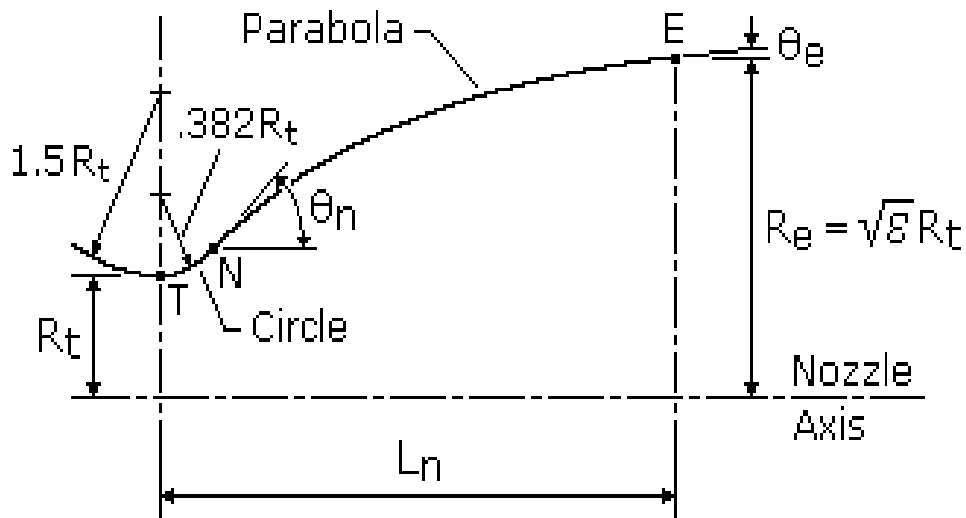


Figure 2.11 Basic design and variables for a parabolic nozzle (Raiano 2013)

This experimental study considers the following nine basic designs for parabolic shaped nozzles:

#### **2.5.2.1 Rao Nozzle**

Rao nozzle (Figure 2.12) is widely used in the aerospace industry to release the exhaust coming from the gas chamber. The main reason to create this nozzle was to get a higher performance nozzle for a shorter length. It is generally about 80% the length of a de Laval nozzle.

#### **2.5.2.2 Modified Rao Nozzle**

This is a Rao nozzle modified to incorporate an elongated throat to observe the effect of throat length (Figure 2.13).

#### **2.5.2.3 Dual Bell Nozzle**

The dual bell nozzle was developed by the aerospace industry to make their rockets more efficient in high altitude conditions. But since in this project the altitude of the nozzle will not be changing, this nozzle would only be tested to note the effect of using this contour on fluid flow. This type of nozzle has two parabolic diverging section instead of one found on a Rao nozzle, as shown in Figure 2.14 (Nürnberg-Genin and Stark 2009).

#### **2.5.2.4 Converging Convex Nozzle**

Design for converging convex nozzle, Figure 2.15, was obtained from a patent of a liquid gas injector in the industry of jet technology. This nozzle has convex circular converging section (Popov et al. 2002).

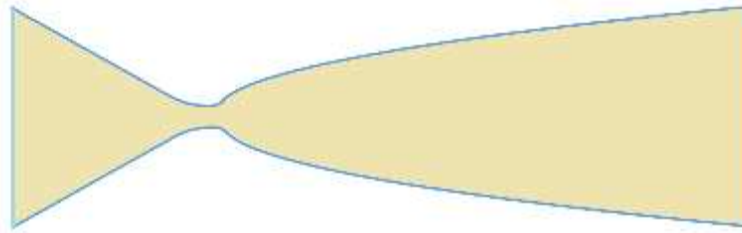


Figure 2.12 Rao nozzle

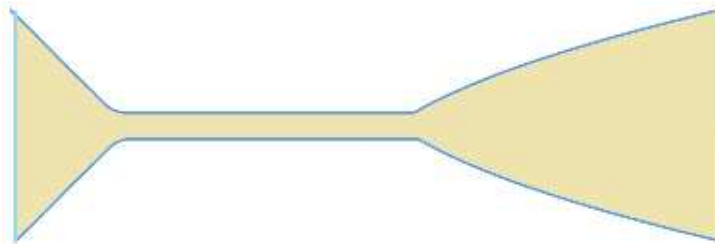


Figure 2.13 Modified rao nozzle

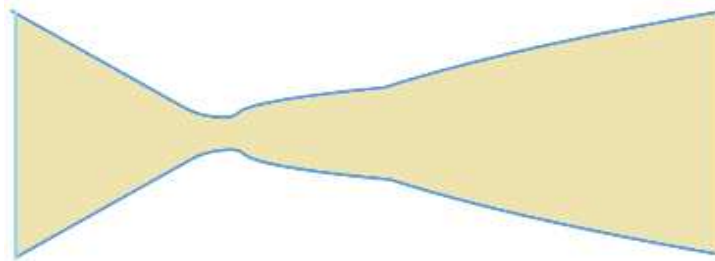


Figure 2.14 Dual bell nozzle

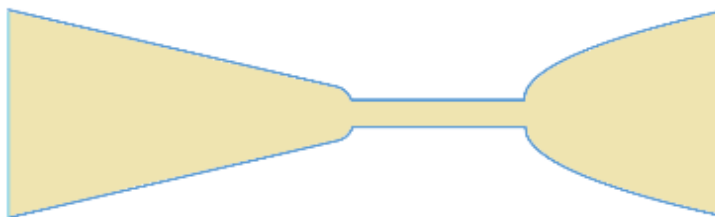


Figure 2.15 Converging convex nozzle

#### **2.5.2.5 Converging Concave Nozzle**

Design for converging concave nozzle (Figure 2.16) was obtained from a patent of a liquid gas injector in the industry of jet technology. This nozzle has a concave circular converging section that extends all the way to the entrance radius (Popov et al. 2002).

#### **2.5.2.6 Moby Dick Nozzle**

This nozzle was developed in the nuclear industry as part of the French Nuclear Thermal Hydraulic code. The tests conducted during this research were done to study two phase critical flow conditions of such nozzles (Bestion 1990). This nozzle is a mix of both circular and conical nozzle shape, as shown in Figure 2.17. The converging section is circular convex shape and the diverging section is linear.

#### **2.5.2.7 ASTAR Nozzle**

This nozzle was developed as part of the ‘ASTAR Project’ undertaken by EU (Staedtke et al. 2005). It is a convergent - divergent nozzle, except its contour is more parabolic compared to de Laval nozzle (Figure 2.18). This converging section of this nozzle is divided into two sections –beginning of the nozzle is circular convex shaped section, which is followed by a circular concave shaped section. The diverging section is a parabola.

#### **2.5.2.8 Deich Nozzle**

The Deich nozzle is also a de Laval nozzle, except its converging part is circular and its diverging part is parabolic (Figure 2.19). Another difference for this nozzle is its small divergent angle of 8 degrees (Ashwood and Higgins 1957).

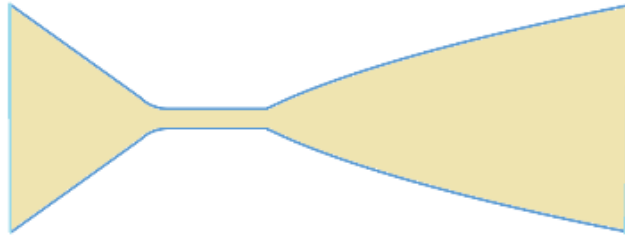


Figure 2.16 Converging concave nozzle

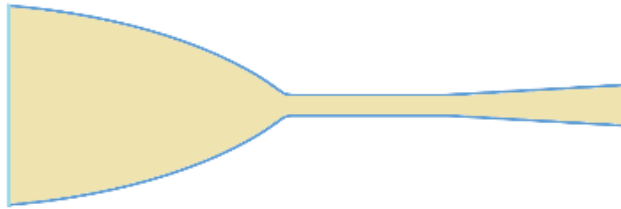


Figure 2.17 Moby dick nozzle

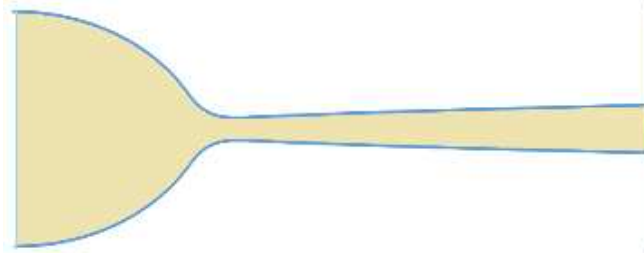


Figure 2.18 ASTAR nozzle

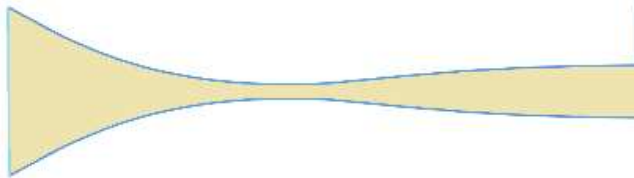


Figure 2.19 Deich nozzle

### 2.5.2.9 LJ Nozzle

The LJ, Luis-Jagmit nozzle, shown in Figure 2.20 was created as part of this work, after 26 nozzle geometries had been tested on the single-phase horizontal facility. This geometry is very similar to one of the ASTAR nozzle geometry except it had longer linear converging and diverging sections.

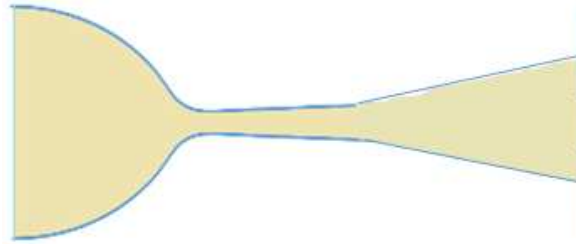


Figure 2.20 LJ nozzle

There exist a lot of physical geometrical parameters and testing variables that can affect the performance of the nozzle. These include:

- Expansion ratio, which is the ratio of exit area to throat area
- Contraction ratio, which is the ratio of inlet area to throat area
- Throat length to throat diameter ratio
- Downstream to upstream pressure ratio
- Heat transfer
- Cone diverging half-angle
- Nozzle angle

All of these factors are dependent on each other in one way or more. The expansion ratio is an important value because knowing this value can help determine the ideal throat length to throat diameter ratio for bell nozzles or conical nozzles, nozzle angle and exit angle for parabolic nozzles (Sutton and Biblarz 2001).

As mentioned above, in a study conducted by Jet Propulsion Lab at NASA it was determined that an optimum nozzle has an elongated throat. In another study conducted a range of 0.2-7 was determined for ideal values of ratio  $L_t/D_t$  (Xue et al. 2002). And if the throat diameter is known, the ideal throat length can be back calculated and the nozzle can be sized accordingly (Elliot and Weinber 1968).

## CHAPTER 3

### METHODOLOGY

This chapter will discuss the methodology that was followed and the experimental setups that were built to achieve the objectives of this research study. Following is the order of the main research tasks:

1. Determine minimum nozzle throat size required to achieve critical flow.
2. Design experimental matrix based on possible nozzle geometries.
3. Create drawings and 3D print nozzle geometries.
4. Design and build experimental facility for single and two-phase horizontal flow testing.
5. Design and build experimental facility for two-phase vertical flow testing.

#### 3.1 Nozzle Throat Size

The first step of this project was to determine the optimum choke diameter that would guarantee critical flow, based on the available gas and liquid flow rates and pressure limitations. In order to do so, the Ashford-Pierce equation (Ashford and Pierce 1975) was used to calculate the critical pressure ratio for varying GLRs.

The liquid flowrate was varied from 15-45 GPM and the gas flowrate was varied from 27-74 CFM. The resulting GLRs were within the range 77-632 CFM/CFM. To calculate the critical pressure ratio for different GLRs, the following nonlinear equation was used:

$$1 = \frac{\frac{R}{n} \left[ \frac{Rn}{n-1} \left( 1 - \epsilon_c^{\frac{n-1}{n}} \right) + (1 - \epsilon_c) \right]}{0.5 \left[ 1 + R \epsilon_c^{\frac{1}{n}} \right]^2 \epsilon_c^{\frac{n+1}{n}}} \quad (3.1)$$

The bisection method was used to solve for the critical pressure ratio,  $\epsilon_c$ . A critical pressure ratio of 0.4846 - 0.4866 was obtained. The average of these two numbers was taken and the critical pressure ratio was determined to be 0.4856.

Next, Pipesim (a static multiphase flow simulator) was used to determine the optimum throat size of the choke considering the given conditions. A simple two-phase model of 1.5 in. pipeline system with a choke was created using Pipesim. Based on the considered GLRs and choke sizes, the pressure drop across the throat was determined as shown in Figure 3.1.

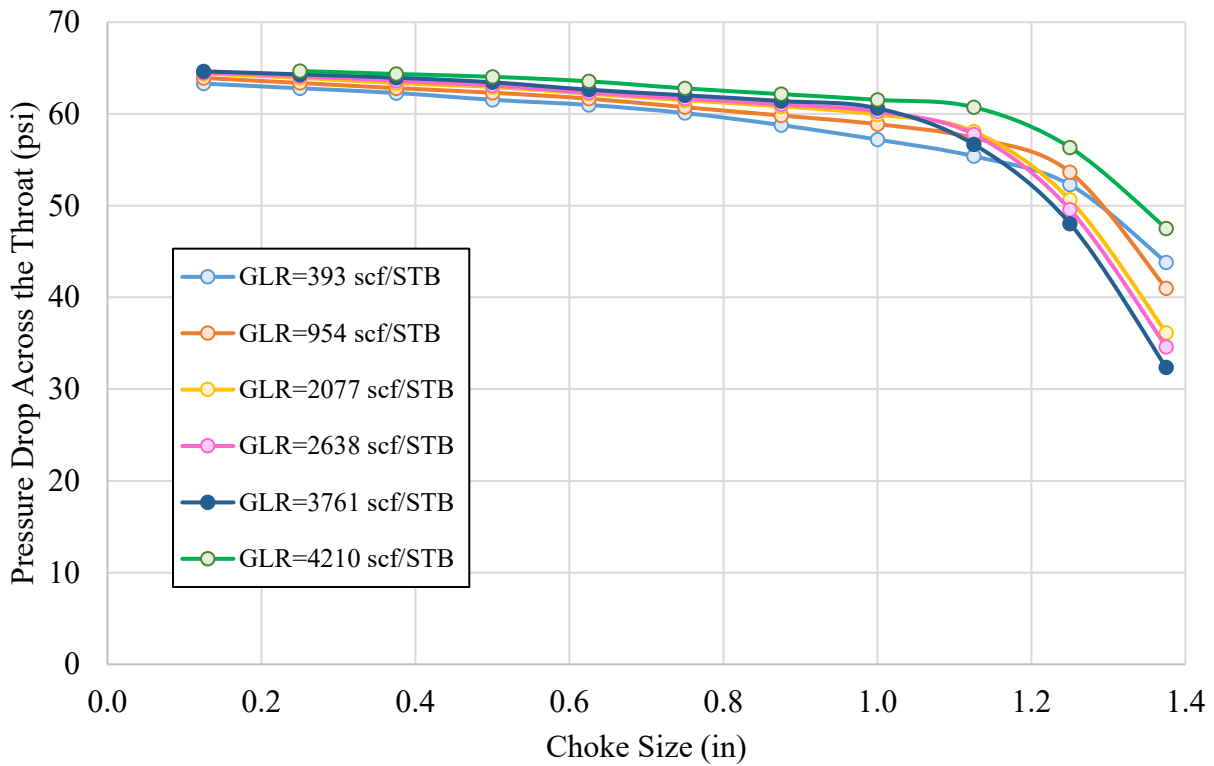


Figure 3.1 Results of pressure drop across choke as choke size and GLRs are varied

By knowing the pressure drop and fixing the upstream inlet pressure to 80 psi, the downstream/upstream pressure ratio was calculated. This ratio was then plotted against the choke sizes for the GLRs considered as shown in Figure 3.2. The red line marks the critical pressure ratio as calculated using Equation (3.1). This plot shows that for a choke size below 1.3 in., the

flow would be critical for all GLRs being considered. However, due to limitations regarding the capability of the compressor being used in the experimental facility, the gas flowrate was limited to 160 scfm. Based on this information Figure 3.3, a plot of gas flowrates against choke size was generated.

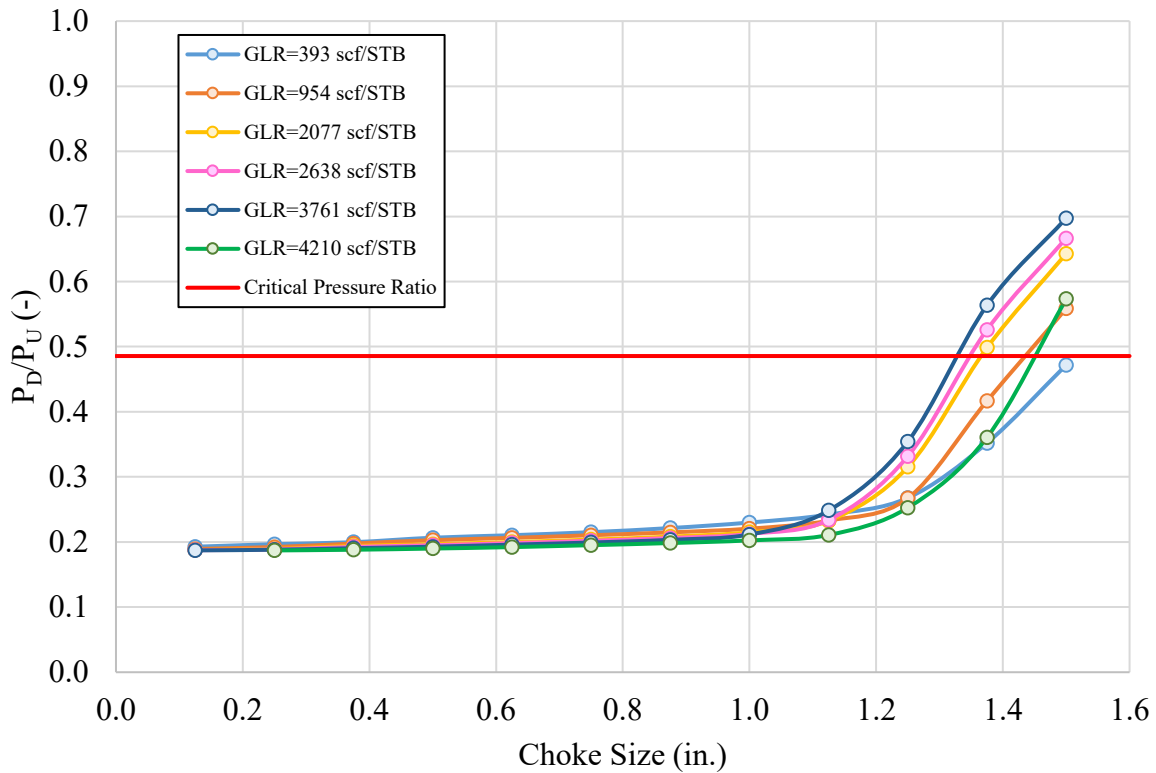


Figure 3.2 Pressure ratio as function of choke size, compared with estimated critical pressure ratio to identify chokes sizes that would provide choked flow at different GLRs

Any choke size in this flowrate would result in critical flow. Ideally, it would be best to pick the least choke size of 0.125 in. This would result in the most optimum critical flow. However, it was determined that this size was too small for practical field applications. So, the throat size was increased to 0.25 in. The throat size of 0.25 in. is a safe approximation even though the calculations were performed using equations for determining choke diameter. Even at very low gas flowrates, critical flow can be observed.

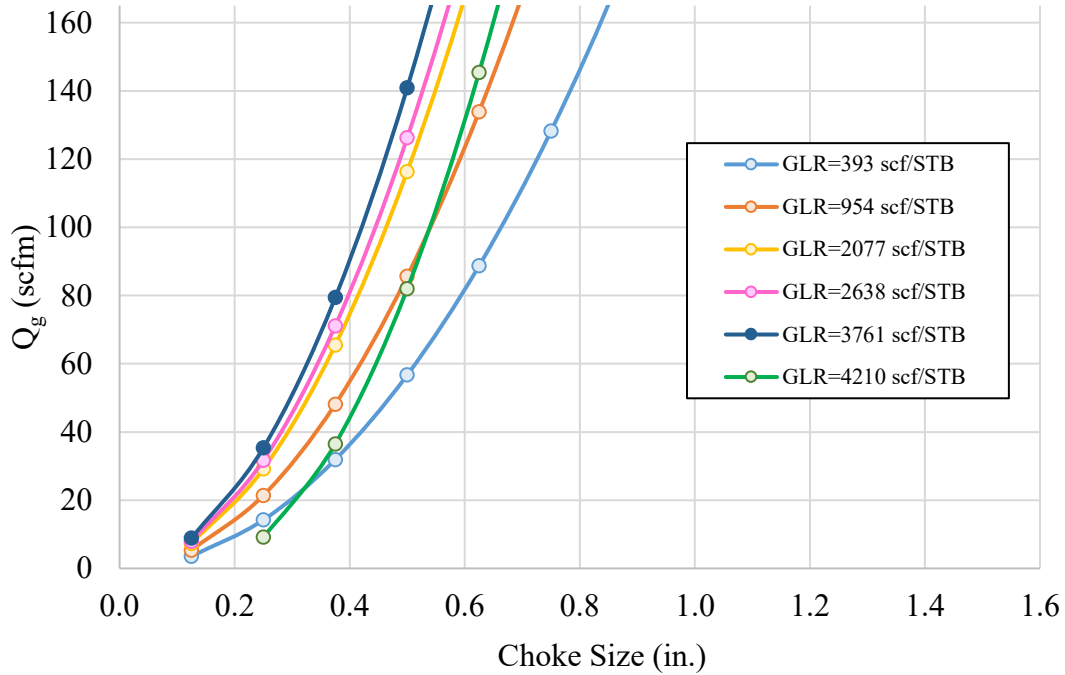


Figure 3.3 Gas flow rate as function of choke size, for selecting choke size based on available gas flowrate

### 3.2 Experimental Matrix

As mentioned in the previous chapter, nozzle performance can be affected by a lot of different variables and parameters. In order to determine the optimum nozzle design, multiple values of each of these geometry parameters were used to create variations of the considered nozzle types. In total, 49 nozzle configurations were available for testing. But after initial testing it was determined that it was not necessary to test all available geometries. Therefore, only 27 out of the 49 nozzle geometries were tested. Table 3.1 details the values of the parameters used to create these nozzle geometries. Parameters varied to create these different geometries include converging angle, diverging angle and throat length.

Table 3.1 Nozzle Geometries Created to Conduct Single-Phase and Two-Phase Experiments by Varying Design Parameters

Nozzle Type	Name	Nozzle number	Converging Angle (°)	Diverging angle (°)	Convergent Length (in)	Throat Length (in)	Divergent Length (in)
Conical	Group 1 Nozzle	2	45	8	0.63	0.00	3.82
		3	45	12	0.63	0.00	2.92
		4	45	10	0.63	0.00	2.32
	Group 2 Nozzle	1	45	8	0.63	0.50	4.45
		2	45	8	0.63	1.75	4.45
	Group 3 Nozzle	1	84	8	0.56	0.00	4.44
Parabolic	Rao Nozzle	1	45	30	0.70	0.00	1.87
		3	45	60	0.70	0.00	1.87
		4	45	90	0.70	0.00	2.01
		5	45	45	0.70	0.00	1.87
	Modified Rao Nozzle	3	45	30	0.70	0.50	1.87
		7	45	60	0.70	0.50	1.87
		8	45	60	0.70	1.75	1.87
	Dual Bell Nozzle	1	45	30/30	0.70	0.00	1.63
	Convex Nozzle	1	30	30	3.16	0.40	1.87
	Concave Nozzle	1	40	30	1.34	0.50	1.87
		2	40	60	1.34	0.50	1.87
	Moby Dick Nozzle	1	45	7	1.17	0.50	0.59
		4	45	7	0.94	1.50	1.76
		2	45	12	0.94	0.50	0.59
	ASTAR Nozzle	1	30	3	1.15	0.00	2.22
		2	30	10	1.15	0.00	2.37
		3	30	15	1.15	0.00	2.47
Deich Nozzle	1	36	8	1.67	0.00	2.08	
	2	36	8	1.67	0.50	1.25	
	3	36	8	1.67	1.75	1.25	
LJ Nozzle	1	30	3	0.68	0.00	5.34	

For horizontal single-phase testing, the upstream pressure, downstream pressure and upstream gas flowrate will be recorded in order to determine the critical pressure ratio and the pressure drop across the nozzle. This gives a resulting experimental matrix of 71 points. For two-phase experiments, the same parameters as single-phase will be recorded, but for six nozzle geometries. This gives an experimental matrix of 18 points.

### **3.3 Nozzle geometry drawing and 3D Print**

3D printing, additive manufacturing technique, was used for building the nozzle geometries. The 3D printer available at Colorado School of Mines, Stratasys Eden 260 VS 3D Printer, was used to print these nozzles. The material used for printing was Vero White Resin. Basic profile designs of these nozzles were created on Microsoft Excel as shown in Figure 3.4, using linear, parabolic and circular equations. The 3D model drawing that was required for 3D printing was created on Solidworks as shown in Figure 3.5. Once these drawings were successfully created, the models were 3D printed as shown in Figure 3.6. The holes on the nozzle are for pressure transducers to be installed across the nozzle body. The number of holes for pressure transducers varied based on the space available on the nozzle body. The threads required to screw the pressure transducers into these holes were 3D printed as part of the nozzle body. The holes and threads were designed accordingly to fit the 0.25 in. pressure transducers and seal the holes. Both ends of the nozzle body consisted of sections that could be glued to 1.5 in. ID PVC unions.

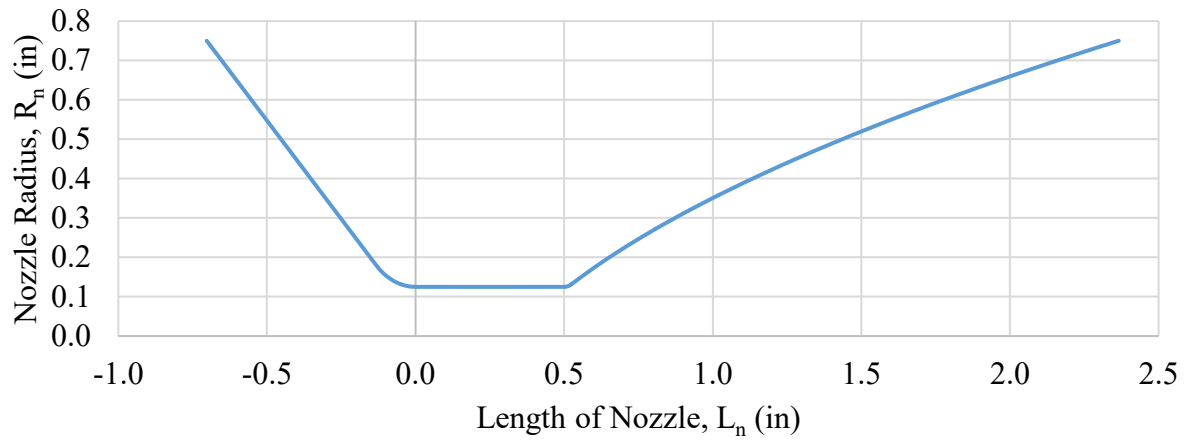


Figure 3.4 Contour profile of a modified rao nozzle created using MS Excel

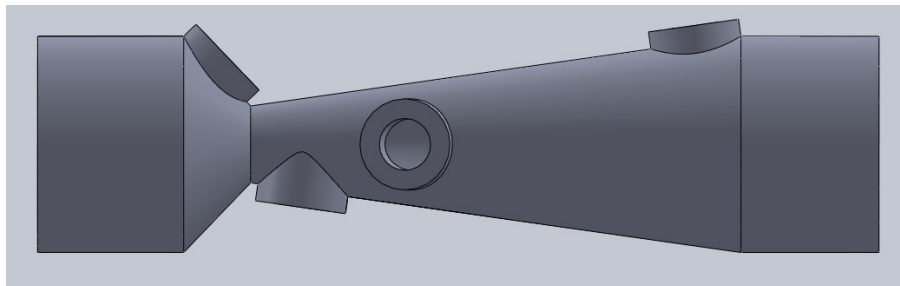


Figure 3.5 Solidworks drawing of converging – diverging conical nozzle

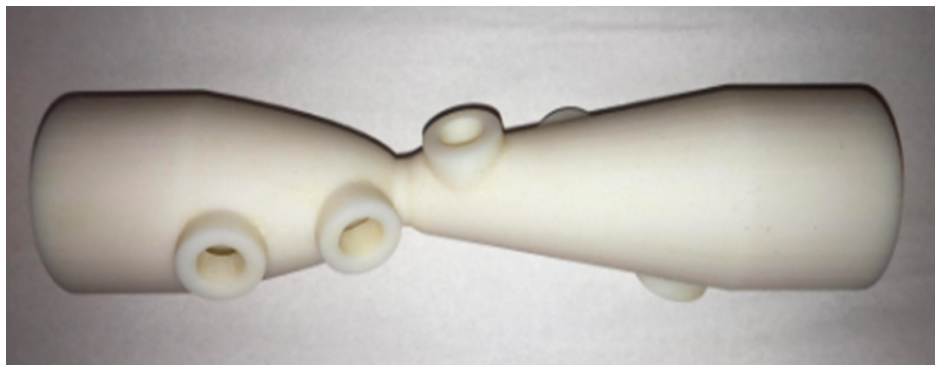


Figure 3.6 3D printed model of a converging diverging nozzle

To ensure that the 3D printed parts could withstand the burst pressure that they will experience, pressure tests were conducted on one nozzle to ensure that the part can withstand pressures of up to 90 psi. A gas compressor was used to flow gas through the nozzle body and the pressure was regulated using a pressure regulator. The procedure for the pressure test was as follows:

- Make connection from the gas line to the nozzle.
- Place nozzle inside a 4 in. thick, clear PVC pipe and plug the nozzle end.
- Submerge the assembly in a water bath.
- Cover the tub with a clear plexiglass.
- Supply pressure to the assembly through the gas line at an increment of 5-10 psi every 3 minutes (Figure 3.7).
- End the test either if bubbles appear at any point or if the pressure reaches 90 psi.

Pressure tests were conducted successfully and there was no leakage from the nozzle body due to burst pressure.

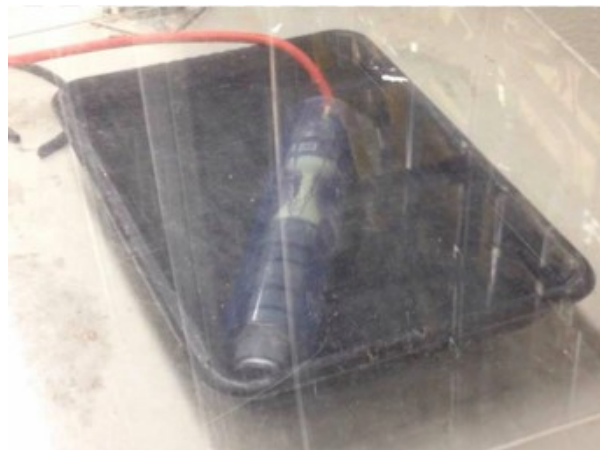


Figure 3.7 Burst pressure test setup to determine the integrity of the 3D printed nozzle and ensure that it can withstand the pressures applied during experiments

### 3.4 Horizontal Facility Setup

A horizontal facility was setup to conduct both single-phase and two-phase testing. The objective of the single-phase experiments is to narrow down the nozzle geometries to a subset of optimum performers. First the facility was constructed just to perform single-phase gas testing (Figure 3.8). Nozzle was installed on a 1.5 in. ID PVC pipe and air was flown from the compressor into the pipe system. This air was vented out at the end of the pipeline facility to the atmosphere. Pressure and temperature transducers were installed along the pipelines. In total, there were Rosemount 10 pressure transducers (PT) and 3 temperature transducers (TT) installed all together. One PT and TT were installed right after the point of gas injection to determine the pressure and temperature at which gas entered the system. Pressure and temperature were measured upstream and downstream the nozzle to determine if the flow was under critical or subcritical flow. At most, seven PTs were installed on the nozzle itself to measure the pressure drop as the fluid flows through it. A Vortex flowmeter was installed upstream of the nozzle in order to measure the gas flow rate. Two control valves were installed as part of the facility – first control valve was used to control the inlet gas pressure and the second control valve was installed at the end of the pipeline to control the back pressure.

Following procedure was followed to perform single-phase horizontal testing:

- Open the supply of air to the inlet of pipeline and to the air tank.
- Open both the gas control valve and the back-pressure valve to 100%.
- Wait 30 minutes for the flow to stabilize. During this time, use spray bottle containing a mixture of water and soap and spray the nozzle to determine any leaks. If leaks are found, restart the experiment after leaks are fixed. If not, continue to next step.
- After 30 minutes, record data from DeltaV system.

- Close backpressure valve by 10% every 5 minutes and until the upstream gas flowrate starts to decrease. Also record data every 5 minutes. Continue opening/closing the valve until the critical point is determined (point where the upstream gas flowrate is no longer constant).
- Shut off air supply.

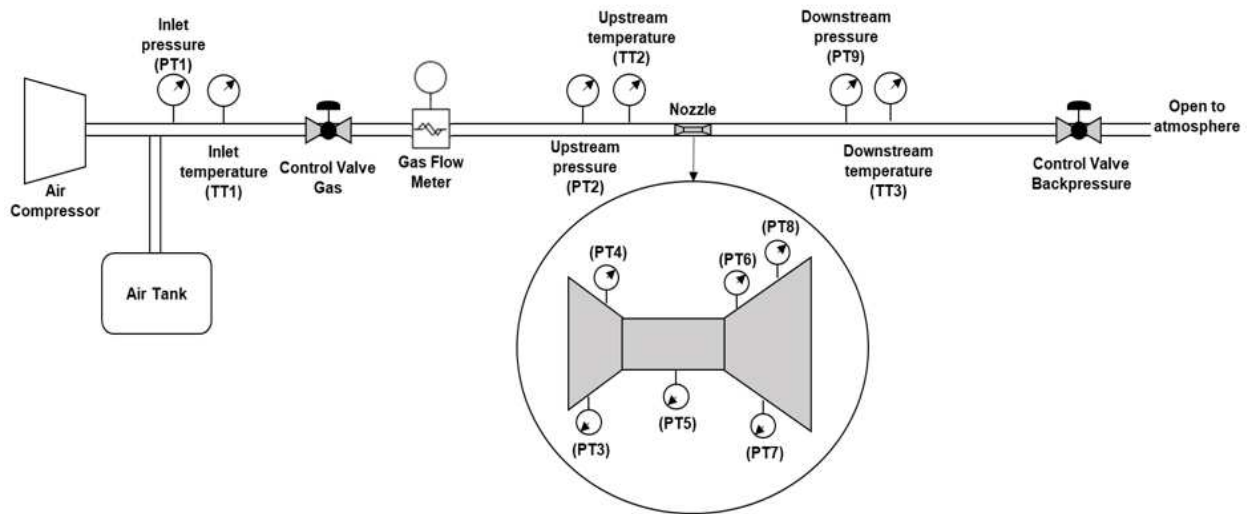


Figure 3.8 Single-phase horizontal flow facility schematic

For two-phase testing, the gas flow set-up remained the same, but some add-ons were made to flow water through the same facility (Figure 3.9). The objective of this experiment was to test the subset of optimum performer nozzles from the single-phase experiments. A third control valve was installed to control the pressure of water entering the system. A magnetic flowmeter was used to measure the flow of water through the pipeline. A PT was installed upstream of control valve to determine the pressure of water flowing through. The system was turned into a flow loop by connecting the tank that holds the discharge water to the tank that supplies the water. Nozzle was attached 15 in. downstream of the mixing point of air and water.

Following procedure was followed to perform two phase horizontal testing:

- Open the supply of air to the inlet of pipeline and to the air tank and turn on the water pump.
- Open both the gas control valve and the back-pressure valve to 100% and the water control valve to 5%.
- Wait for 30 minutes for the flow to stabilize.
- Close backpressure valve by 10% every 10 minutes and until the upstream gas flowrate starts to decrease. Continue opening/closing the valve until the critical point is determined.
- Shut off air supply and pump.
- Record data from DeltaV system.

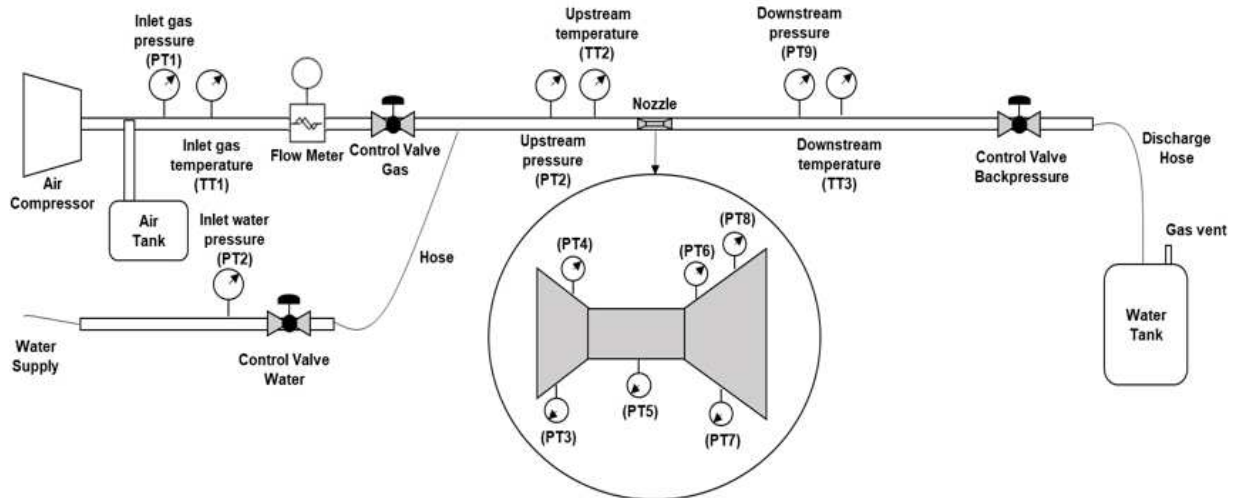


Figure 3.9 Two-phase horizontal flow facility schematic

### 3.5 Vertical Facility Setup

Experiments to determine the effect of varying nozzle profiles as an artificial lift system were carried out in a small-scale vertical experimental facility flow loop. The nozzle was installed on a 1.5 in. ID PVC pipe and the fluids were discharged through a 2 in. ID PVC pipe. The objective of this experiment was to determine the optimum nozzle design that can maximize downstream/upstream pressure ratio and minimize pressure drop across the nozzle as the fluid flows through its profile. This facility consists of a flow loop that comprises of a 1.5 in. ID and 30 ft long vertical production section and a 2 in. and 25 ft long vertical discharge section. There also exist three lateral sections in this flow loop – first is the water line section from where water is supplied to the vertical production pipe; second is the gas line section from where gas is supplied to the vertical production pipe; third there is a lateral discharge section that connects the vertical discharge line to the tank. All the lateral and vertical sections are made of clear PVC pipe to observe the flow through the loop. The nozzle was on the vertical production line, at a distance of 2 ft above gas and water mixing point. This was done to allow enough pipe length upstream of the nozzle for the flow to be fully develop before it entered the nozzle.

Pressure and temperature along the flow loop were measured using Rosemount PTs and TTs, respectively. 12 PTs and 3 TTs were located throughout the loop. Pressure and temperature were measured upstream and downstream the nozzle in order to determine if the flow was under critical or subcritical condition. Pressure and temperature were in the gas line and only pressure was measured in the water line. At most, seven PTs were on the nozzle itself in order to measure the pressure drop as the fluid flows through it.

In this facility, three control valves and two flowmeters were installed. One control valve was on the water injection line, the second control valve was installed on the gas injection line in

order to control the pressure of water and gas entering the nozzle and the third control valve was on the top of the vertical pipe, to control the downstream pressure. A Vortex flowmeter was used to measure the gas mass rate and a Magnetic flowmeter was used to measure the water mass rate. Compressed air was used as the gas phase, and was supplied from a rotary screw air compressor. Tap water was used as the liquid phase and pumped from a 130-gallon water tank by a centrifugal pump. After flowing through the test section, fluids were sent to a second water tank where the downstream water flow rate and cumulative production were measured. The second water tank was placed on a weighing machine to measure the weight of water that is being collected in the tank throughout the experiment (Figure 3.10).

Following procedure was followed in order to perform two-phase vertical testing:

- Open the supply of air to the inlet of pipeline and to the air tank and turn on the water pump.
- Open both the gas control valve and the back-pressure valve to 100% and the water control valve to 5%.
- Wait for an hour for the flow to stabilize.
- After the flow has stabilized, open the valve to allow water to flow into the second water tank. Record the weight of water after the tank has been filling for a minute. Continue to do so for 10 minutes.
- Close backpressure valve by 10% every 10 minutes and until the upstream gas flowrate starts to decrease. Continue opening/closing the valve until the critical point is determined.
- Shut off air supply and pump.
- Record data from DeltaV system.

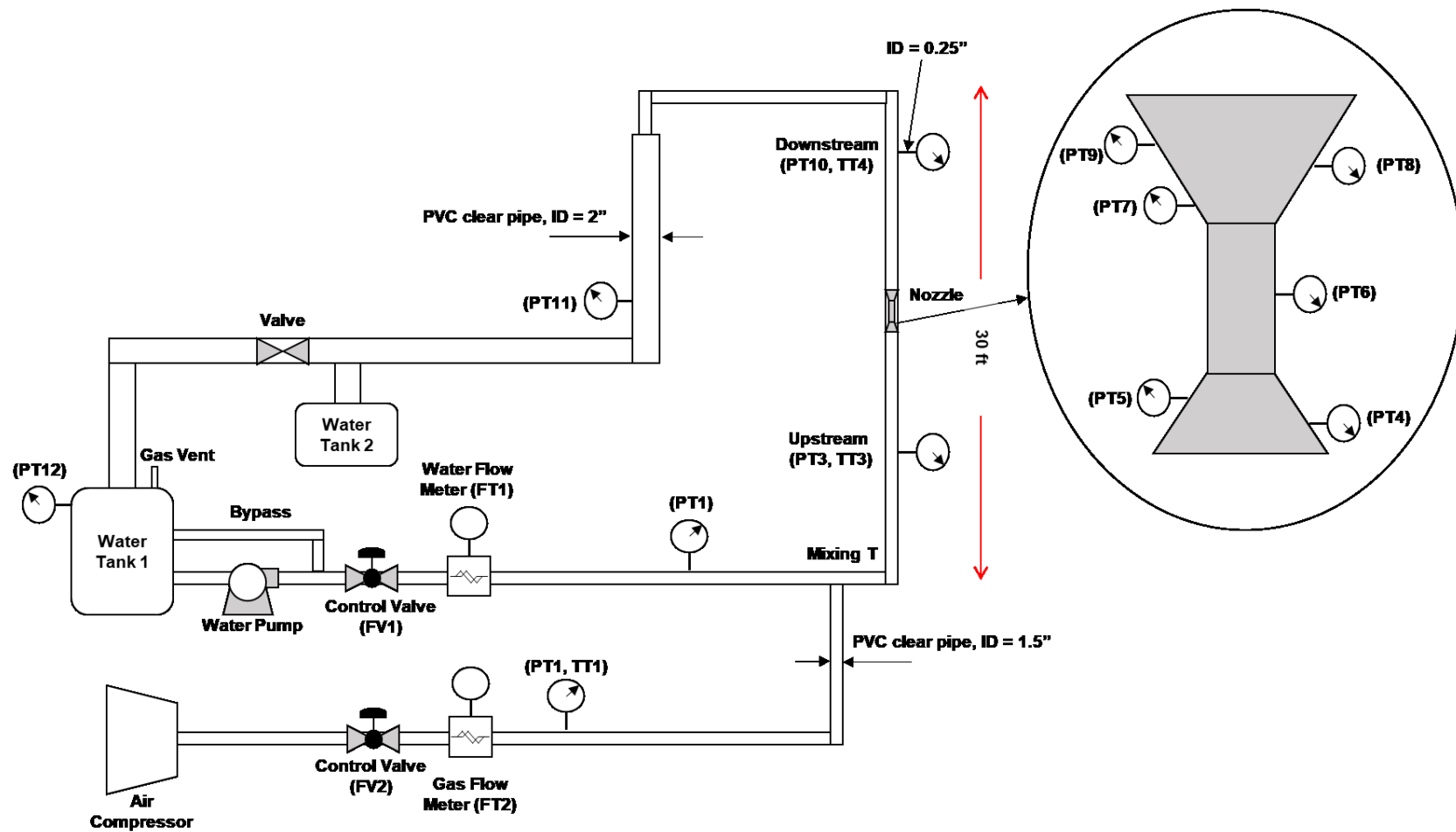


Figure 3.10 Two-phase vertical flow facility schematic

### **3.6 Data Collection**

The PTs, TTs, flowmeters and control valves were connected to a DeltaV system. DeltaV is a distributed control system that helps control the configuration of the control valves and records data from the devices connected to the system. Based on the amperage of current that is being supplied by the devices to the control box, DeltaV scales the values based on the end points that the devices are configured for in the system and provides an output value. The control box consists of analog inputs and analog output cards that transfer signal back and forth from the devices to the DeltaV system. This system was used to record data incoming from all the devices and was also used to open or close the control valves.

## CHAPTER 4

### RESULTS AND DISCUSSIONS

In this chapter, the results of single-phase horizontal flow tests, two-phase horizontal flow tests and two-phase vertical flow tests are presented and discussed. Results obtained from single-phase testing were analyzed and geometries from the top performing groups and a base case of a conical shaped nozzle were chosen for further testing in the two-phase horizontal and vertical flow setup. As the optimum geometry types were determined early during single-phase horizontal tests, only configurations of nozzle types that performed well were further tested. Therefore, in total 27 nozzle geometries were experimentally tested. In addition, an empirical model was developed for single-phase flow tests to model the data obtained based on geometrical surface area of nozzles. Data obtained from two-phase horizontal flow tests was analyzed to determine the effect of two-phase flow on nozzle performance such that it altered the ranking of nozzle geometries. Data from two-phase vertical flow tests was analyzed to determine the performance of the optimum nozzle and compare nozzle geometry performance to the horizontal two-phase results.

#### **4.1 Data**

Data obtained after testing each nozzle was organized and assessed for the different type of experiments (single and two-phase horizontal flow and two-phase vertical flow). This data included upstream pressure, upstream temperature, downstream pressure, downstream temperature, pressures across nozzle, upstream gas flowrate and upstream water flowrate (for two-phase experiments). Based on these parameters, it was determined at which point did the flow in the nozzle change from critical to sub-critical flow. This was determined by creating a

plot as shown in Figure 4.1. On the x-axis, ratio of downstream pressure to upstream pressure is plotted and on the y-axis the upstream gas flowrate is plotted. The point at which the flow goes from critical to sub-critical is called the critical pressure point. This point occurs when the upstream flowrate is not constant anymore. The critical (choked) region and sub-critical region are marked on the plot. Another series in the same plot is the pressure drop across nozzle against the downstream to upstream pressure ratio.

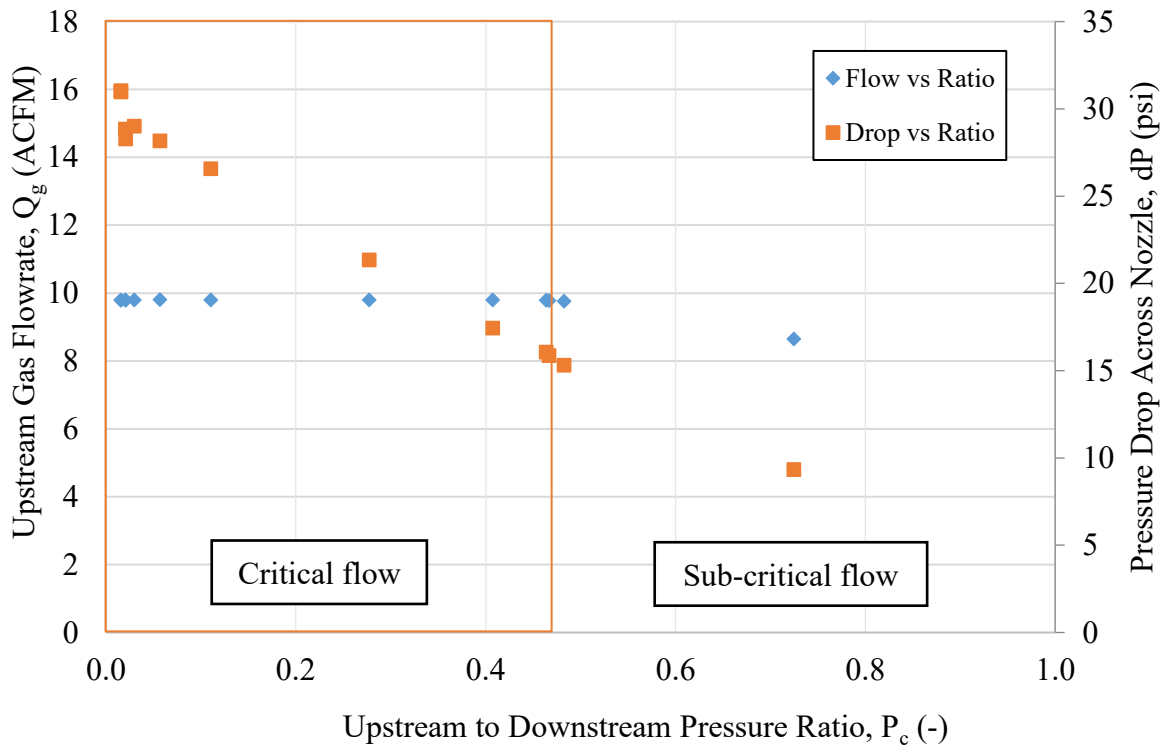


Figure 4.1 Identify critical pressure point and pressure drop across nozzle

Such plots were created for all the nozzles that were tested as part of both single-phase and two-phase tests to identify the critical pressure ratio and visualize the pressure drop across the nozzle. Table 4.1 shows the pressure drop and critical pressure ratio for every nozzle tested in the single-phase horizontal setup, along with respective upstream gas pressure and flowrate.

Table 4.2 shows the same data for nozzles tested in the two-phase horizontal flow setup and Table 4.3 shows data for nozzles tested in two-phase vertical flow setup.

Table 4.1 Single-Phase Horizontal Flow Experimental Results

Nozzle		Pressure Drop, dP (psi)	Critical Pressure Ratio, $P_c$ (-)	Upstream Pressure, $P_u$ (psig)	Upstream Gas Flowrate, $Q_{u,g}$ (ACFM)	
Conical	Group 1	Nozzle 2	13.1	0.30	18.7	12.9
		Nozzle 3	15.6	0.24	20.6	12.6
		Nozzle 4	15.4	0.36	24.1	12.2
	Group 2	Nozzle 1	15.6	0.34	23.6	12.4
		Nozzle 3	18.4	0.45	30.0	9.8
	Group 3	Nozzle 1	9.3	0.57	21.8	13.0
Parabolic	Rao Bell	Nozzle 1	11.6	0.18	15.1	16.6
		Nozzle 3	14.4	0.33	21.6	12.7
		Nozzle 4	12.8	0.31	16.6	13.0
		Nozzle 5	13.6	0.44	24.3	12.3
	Modified Rao Bell	Nozzle 3	17.4	0.21	22.0	11.9
		Nozzle 7	20.0	0.24	26.3	11.3
		Nozzle 8	18.3	0.44	24.3	10.2
	Dual Bell	Nozzle 1	12.7	0.43	22.4	12.7
	Convex Bell	Nozzle 1	15.1	0.41	25.6	11.8
	Concave Bell	Nozzle 1	21.0	0.22	26.2	11.4
		Nozzle 2	16.4	0.28	22.9	11.4
	ASTAR	Nozzle 1	6.0	0.75	23.8	12.3
		Nozzle 2	9.8	0.58	21.2	12.9
		Nozzle 3	10.2	0.48	19.6	12.7
	Moby Dick	Nozzle 1	11.3	0.49	21.9	11.9
		Nozzle 2	14.5	0.34	22.0	11.7
		Nozzle 4	13.4	0.50	26.3	10.1
	Deich	Nozzle 1	12.3	0.53	25.9	11.5
		Nozzle 2	12.6	0.54	27.5	10.9
		Nozzle 3	14.9	0.56	33.8	9.2
	LJ	Nozzle 1	7.9	0.65	22.2	12.0

Table 4.2 Two-Phase Horizontal Flow Experimental Results

Nozzle			Critical Pressure Ratio, $P_c$ (-)	Pressure Drop, $dP$ (psi)	Upstream Pressure, $P_u$ (psig)	Upstream Gas Flowrate, $Q_{u,g}$ (ACFM)
Conical	Group 1	Nozzle 4	0.44	18.5	33	8.6
Parabolic	ASTAR	Nozzle 1	0.50	20.8	41	8.0
		Nozzle 2	0.54	16.4	36	8.0
	Moby Dick	Nozzle 1	0.43	21.7	38	7.7
	Deich	Nozzle 1	0.42	27.5	48	6.6
	LJ	Nozzle 1	0.36	24.9	39	7.4

Table 4.3 Two-Phase Vertical Flow Experimental Results

Nozzle			Critical Pressure Ratio, $P_c$ (-)	Pressure Drop, $dP$ (psi)	Upstream Pressure, $P_u$ (psig)	Upstream Gas Flowrate, $Q_{u,g}$ (ACFM)
Conical	Group 1	Nozzle 4	0.29	23	32	9.3
Parabolic	ASTAR	Nozzle 1	0.40	20	34	9.0
		Nozzle 2	0.44	17	30	8.9
	Moby Dick	Nozzle 1	0.30	27	39	7.6
	Deich	Nozzle 1	0.32	24	36	8.3
	LJ	Nozzle 1	0.41	23	39	7.6

#### 4.2 Data Analysis – Single-Phase Horizontal Flow

In order to determine which nozzle configurations performed better than others, the nozzle geometries were ranked separately based on the critical pressure ratio (Table 4.4) and pressure drop across nozzle (Table 4.5, Pg. 50) at critical pressure point. Six best performing nozzles in each case (highest critical pressure point and lowest pressure drop across nozzle) are highlighted. It can be observed that the nozzles that have a high critical pressure ratio point, do not necessarily have the least pressure drop across the nozzle. This could be due to different

upstream pressures and gas flowrates that the nozzles tested at. Table 4.6 (Pg.51) compares nozzles based on both above mentioned criteria and highlights the optimum nozzles.

Table 4.4 Ranking of Nozzle Performance Based on Critical Pressure Ratio

Rank - Critical Pressure Ratio	Nozzle	Critical Pressure Ratio, $P_c$ (-)
1	ASTAR - Nozzle 1	0.74
2	LJ Nozzle	0.65
3	ASTAR - Nozzle 2	0.58
4	Conical Group 3 - Nozzle 1	0.57
5	Deich - Nozzle 3	0.56
6	Deich - Nozzle 2	0.54
7	Deich - Nozzle 1	0.53
8	Moby Dick - Nozzle 4	0.50
9	Moby Dick - Nozzle 1	0.49
10	ASTAR - Nozzle 3	0.48
11	Conical Group 2 - Nozzle 3	0.45
12	Rao Bell - Nozzle 5	0.44
13	Modified Bell Rao Nozzle 8	0.44
14	Dual Bell - Nozzle 1	0.43
15	Convex Bell - Nozzle 1	0.41
16	Conical Group 1 - Nozzle	0.36
17	Moby Dick - Nozzle 2	0.34
18	Conical Group 2 - Nozzle 1	0.34
19	Rao Bell - Nozzle 3	0.33
20	Rao Bell - Nozzle 4	0.31
21	Conical Group 1 - Nozzle 2	0.28
22	Concave - Nozzle 2	0.28
23	Conical Group 1 - Nozzle 3	0.24
24	Modified Rao Bell - Nozzle 7	0.24
25	Concave Bell - Nozzle 1	0.22
26	Modified Rao Bell - Nozzle 3	0.21
27	Rao Bell - Nozzle 1	0.15

Table 4.5 Ranking of Nozzle Performance Based on Pressure Drop Across Nozzle

Rank - Pressure Drop	Nozzle	Pressure Drop, dP (psi)
1	ASTAR - Nozzle 1	6.0
2	LJ - Nozzle 1	7.5
3	Conical Group 3 - Nozzle 1	9.3
4	ASTAR - Nozzle 2	9.8
5	ASTAR - Nozzle 3	10.2
6	Moby Dick - Nozzle 1	11.3
7	Rao Bell - Nozzle 1	11.6
8	Deich - Nozzle 1	12.3
9	Deich - Nozzle 2	12.6
10	Dual Bell - Nozzle 1	12.7
11	Rao Bell - Nozzle 4	12.8
12	Conical Group 1 - Nozzle 2	13.1
13	Moby Dick - Nozzle 4	13.4
14	Rao Bell - Nozzle 5	13.6
15	Rao Bell - Nozzle 3	14.4
16	Moby Dick - Nozzle 2	14.5
17	Deich - Nozzle 3	14.9
18	Convex Bell - Nozzle 1	15.1
19	Conical Group 1 - Nozzle 4	15.4
20	Conical Group 1 - Nozzle 3	15.6
21	Conical Group 2 - Nozzle 1	15.6
22	Concave - Nozzle 2	16.4
23	Modified Rao Bell - Nozzle 3	17.4
24	Modified Rao Bell - Nozzle 8	18.3
25	Conical Group 2 - Nozzle 3	18.4
26	Modified Rao Bell - Nozzle 7	20.0
27	Concave Bell - Nozzle 1	21.0

Table 4.6 Rank of Nozzles Based on Both Critical Pressure Ratio and Pressure Drop

Nozzle			Rank - Pressure Drop	Rank - Critical Pressure Ratio
Conical	Group 1	Nozzle 2	12	21
		Nozzle 3	20	23
		Nozzle 4	19	16
	Group 2	Nozzle 1	21	18
		Nozzle 3	25	11
	Group 3	Nozzle 1	3	4
Parabolic	Rao Bell	Nozzle 1	7	27
		Nozzle 3	15	19
		Nozzle 4	11	20
		Nozzle 5	14	12
	Modified Rao Bell	Nozzle 3	23	26
		Nozzle 7	26	24
		Nozzle 8	24	13
	Dual Bell	Nozzle 1	10	14
	Convex Bell	Nozzle 1	18	15
	Concave Bell	Nozzle 1	27	25
		Nozzle 2	22	22
	ASTAR	Nozzle 1	1	1
		Nozzle 2	4	3
		Nozzle 3	5	10
	Moby Dick	Nozzle 1	6	9
Nozzle 2		16	17	
Nozzle 4		13	8	
Deich	Nozzle 1	8	7	
	Nozzle 2	9	6	
	Nozzle 3	17	5	
LJ	Nozzle 1	2	2	

From this table it can be noted that four nozzle groups performed best when both criteria are taken into consideration - ASTAR, Deich, Moby Dick and LJ. To understand why these nozzle geometries performed better than others, the pressure readings recorded at different locations of the nozzle were studied. Because of the limitations of space on the nozzle body, pressure transducers were located at areas where there was enough room for them to fit. As a result, there are some nozzles with 7 pressure transducers and others with 3 pressure transducers located on them. And nozzles that had no elongated throat region, had no room for pressure transducer at the throat. So, the pressure in the throat could not be recorded. To make the analysis consistent, the nozzle area was divided into four regions as shown in Figure 4.2.

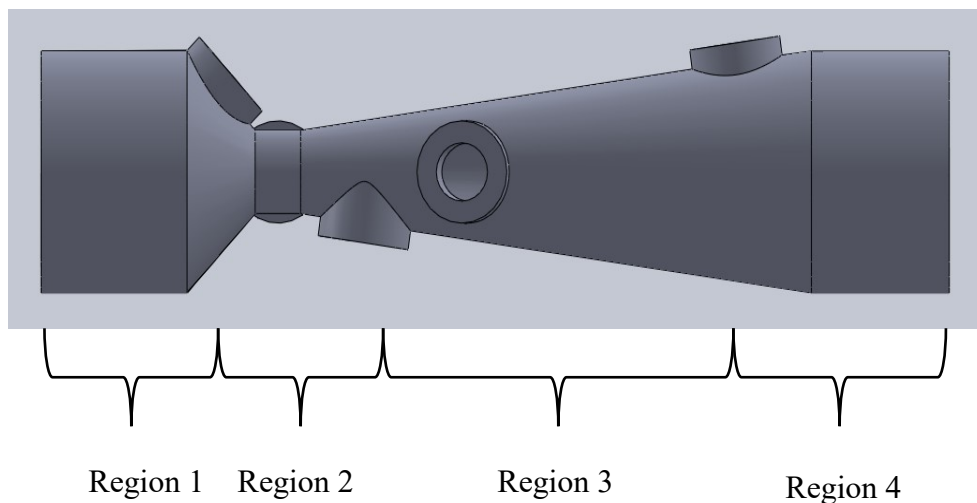


Figure 4.2 Dividing regions of nozzle body for pressure drop analysis

First region includes area from pipe to the convergent section, second region includes area from convergent section to throat to beginning of divergent section, third region includes area from beginning of divergent section to the end of divergent section and the fourth region includes area from the end of divergent section to the pipe area. In addition, the upstream pressure was similar when experiments were performed for different nozzles, but not the same.

So again, to make the analysis consistent, instead of comparing the pressures at different locations for different nozzles, the ratio of pressure at certain location in the nozzle to the upstream pressure was compared.

Figure 4.3 shows the regions and the pressure ratio drop across nozzle. From this figure, it can be noted that the region that has the most impact on the pressure behavior is region 2, which includes the throat. Therefore, the shape of the area right before the throat, the throat and shape of the area right after the throat play a significant role in determining the pressure drop across the nozzle. Figure 4.4 (Pg.55) and Figure 4.5 (Pg.55) show the pressure ratio profile as it changes with flow through nozzle for optimal geometries and non – optimal geometries respectively. From these figures the effect of diverging geometry on pressure recovery can be seen.

There are two main reasons some geometries performed better than the others – 1) pressure drop in region 2, 2) pressure recovery in region 3 region 4. A stark difference can be observed in optimal and non – optimal geometries if these reasons are considered. In case of optimal geometries, the pressure drop in region 2 is not as low as compared to non-optimal geometries. The range of pressure drop ratio right after the throat for optimal geometries is from 0.40 – 0.58. In case of non – optimal geometries, the range is 0.15 – 0.39. Along with this, it can also be observed that the pressure generally recovers in case of optimal geometries because of the shape of the diverging section. This results in a lower overall pressure drop across the nozzle and a higher critical pressure ratio. For the non – optimal nozzles, the velocity is still high in regions 3 and 4 and as a result, the pressure recovery is low. This results in a higher pressure drop across the nozzle and a lower critical pressure ratio.

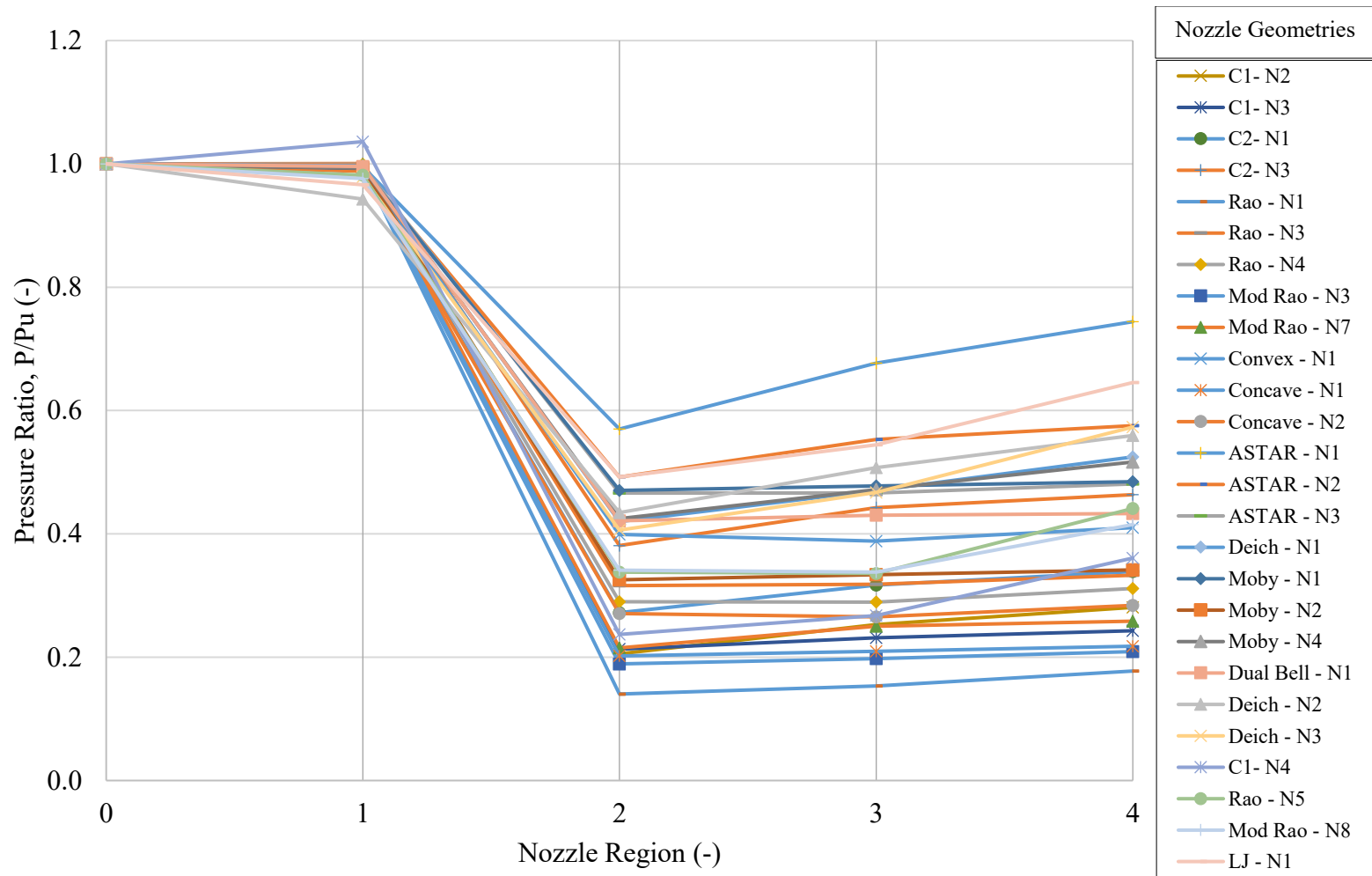


Figure 4.3 Pressure drop ratio across nozzle for single-phase horizontal flow tests

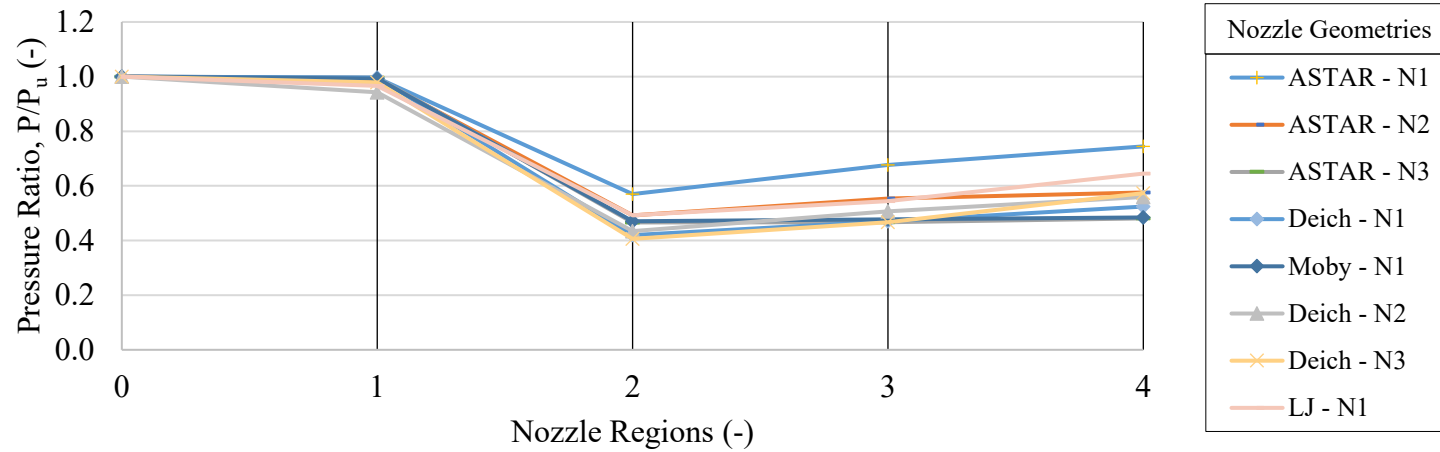


Figure 4.4 Pressure drop ratio of optimal geometries

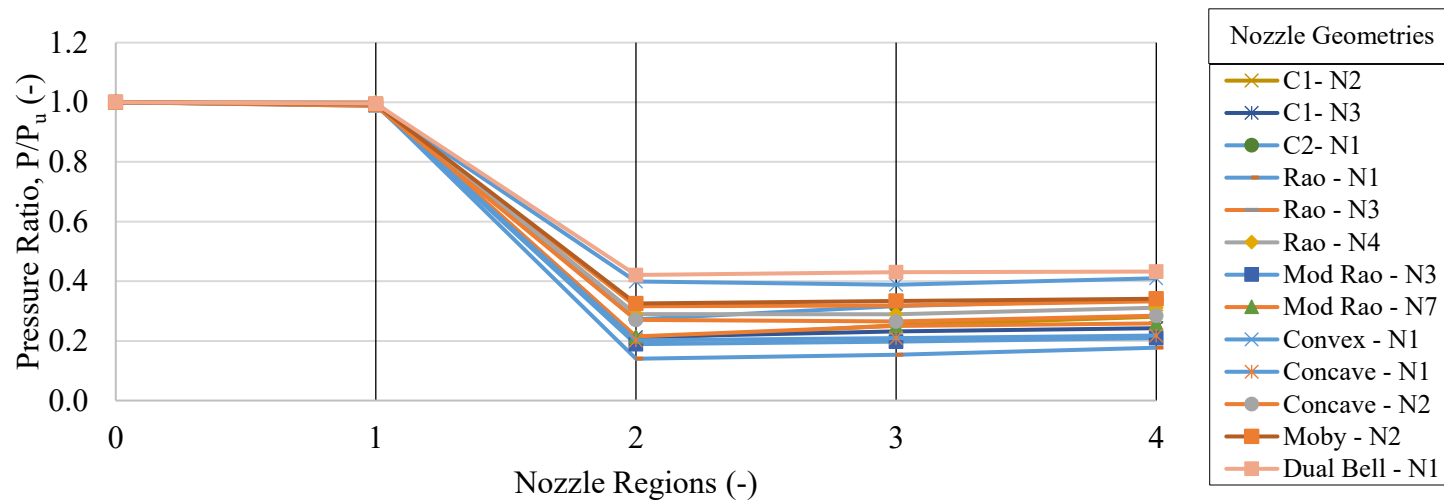


Figure 4.5 Pressure drop ratio of non – optimal geometries

Based on results obtained, the effect of increasing diverging angles, elongating the throat lengths and increasing overall length of the nozzle can be observed among different nozzle groups. The effect of these parameters will be discussed below for the basic conical and parabolic nozzle shapes as the other sub groups of these nozzles followed similar patterns.

By analyzing data from Conical group 1 nozzles, the effect of changing diverging angle in a conical nozzle can be determined. Three different nozzles with diverging angles of  $8^\circ$ ,  $10^\circ$  and  $12^\circ$  respectively were tested. Figure 4.6 shows the results from these tests. It can be noted that the nozzle with the highest critical pressure ratio is the one with a diverging angle of  $10^\circ$ , followed by  $8^\circ$  and  $12^\circ$ . In general, there is a loss of performance that is observed as the diverging angle is increased. Similar trend can be observed in the Moby Dick nozzles, where the diverging section is conical.

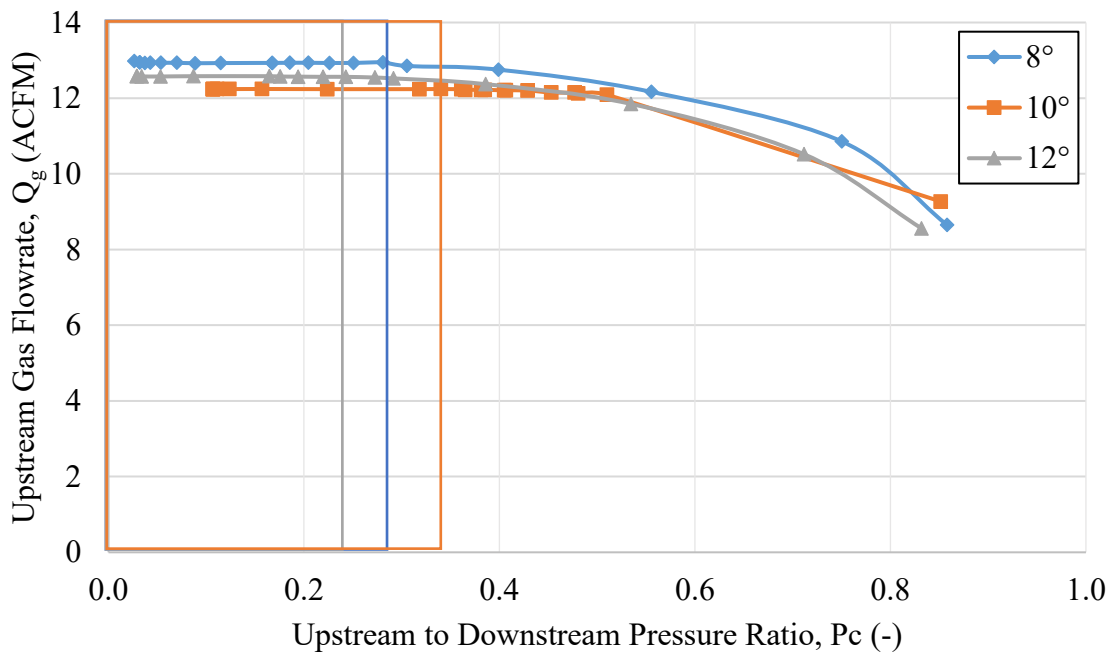


Figure 4.6 Effect of varying diverging angles on nozzle performance for conical shaped nozzles

By analyzing data from Conical group 2 and group 1 nozzles, the effect of elongated throat lengths in a conical nozzle can be determined. Three different nozzles with throat lengths of 0 in., 0.5 in. and 1.5 in. respectively and the same diverging angle of  $8^\circ$  were tested. Figure 4.7 shows the results from this test. A longer elongated throat resulted in a higher critical pressure ratio. However, since the velocity of air is higher for a longer length in nozzles with larger elongated throats, the pressure drop across the nozzle is higher. Similar trends can be observed in Moby Dick nozzles.

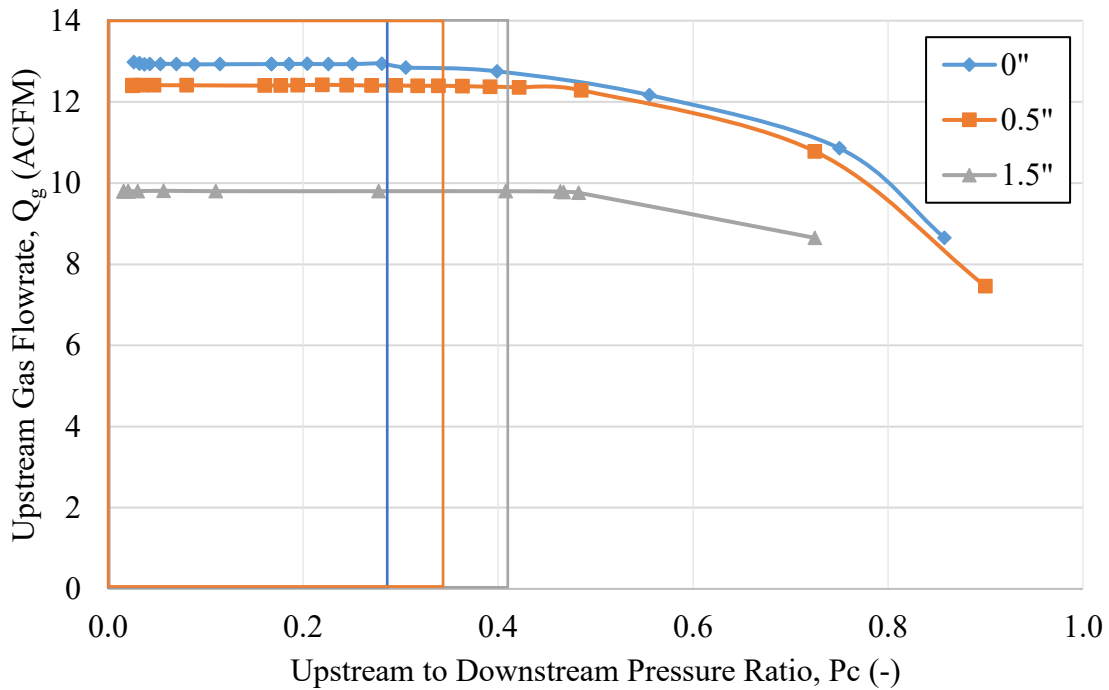


Figure 4.7 Effect of varying throat lengths on nozzle performance for conical shaped nozzles

By analyzing data from Rao nozzles, the effect of changing diverging angles in a parabolic nozzle can be determined. Three different nozzles with diverging angles of  $45^\circ$ ,  $60^\circ$  and  $90^\circ$  respectively were tested. Figure 4.8 shows the results from these tests. It can be noted that similar to conical nozzles, the nozzle with the smallest diverging angle resulted in the

highest critical pressure ratio. A loss of nozzle performance is observed as the diverging angle is increased. Similar trends can be observed in ASTAR nozzles. Another feature of these nozzles is that there is no elongated throat present in the nozzle types. If there is an elongated throat, and the diverging angle is increased, the performance of the nozzle with a higher diverging angle is better. Such trends can be observed in Modified Rao and Concave Bell nozzles.

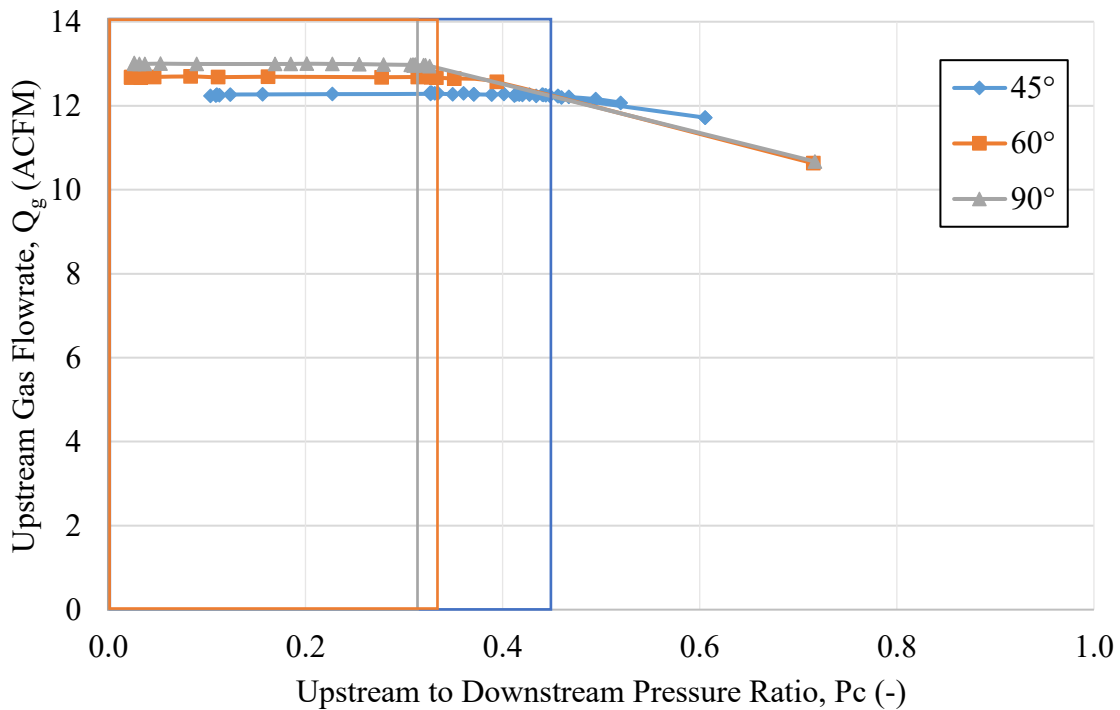


Figure 4.8 Effect of varying diverging angles on nozzle performance for parabolic shaped nozzles

By analyzing data from Modified Rao and Rao nozzles, the effect of different elongated throat lengths in a parabolic nozzle can be determined. Two different nozzles with throat lengths of 0 in. and 1.5 in. respectively and a diverging angle of 60° were tested. Figure 4.9 shows the results from these tests. Nozzle performance in terms of critical pressure ratio increases as length of throat increases, but similar to conical nozzles, the pressure drop across the nozzle increases as well with an increase in throat length. Similar trend can be observed in Deich nozzles,

however the effect of throat length is not too profound as the critical pressure ratio for all three nozzles are very close to each other.

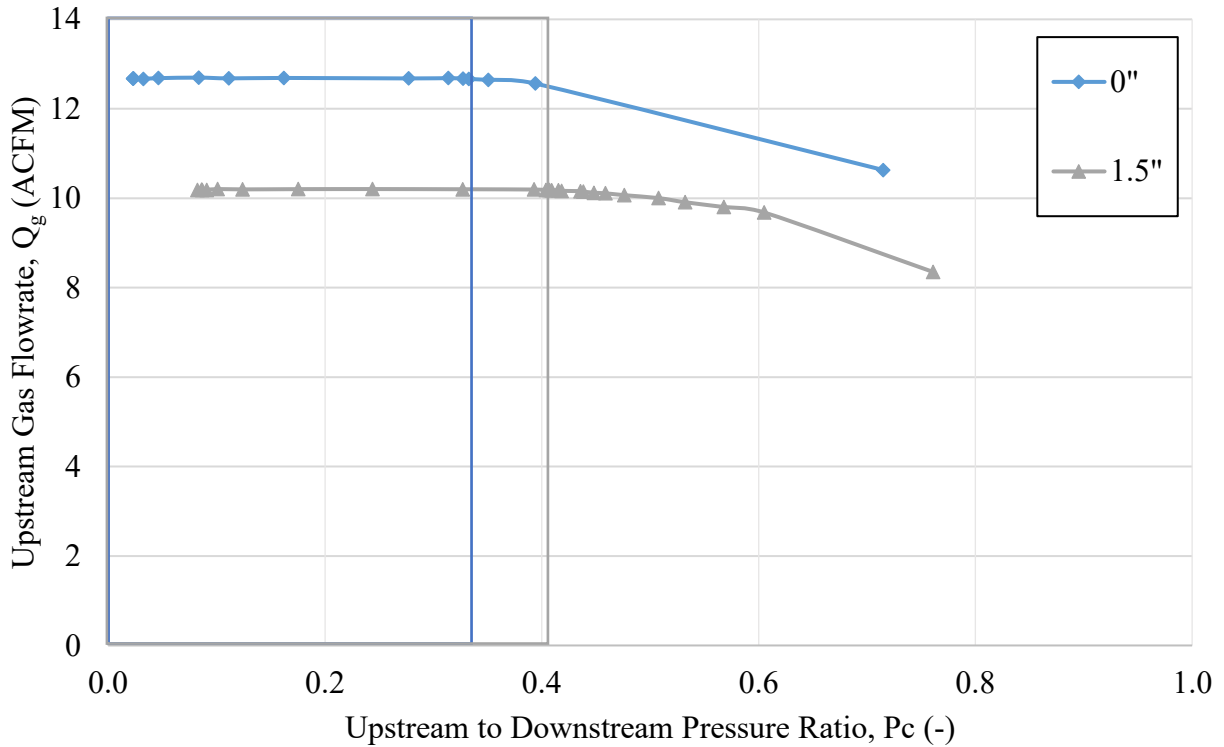


Figure 4.9 Effect of varying throat lengths on nozzle performance for parabolic shaped nozzles

By analyzing the results from ASTAR nozzle 1 and LJ nozzle 1, the effect of total nozzle length on nozzle performance can be determined. Both have similar geometry right before and right after the throat, except LJ nozzle is longer in length compared to ASTAR nozzle. Figure 4.10 shows the results from the test. It can be observed that the critical pressure ratio for both nozzles is very similar. The only difference in performance is that the LJ nozzle has a higher pressure drop across the nozzle.

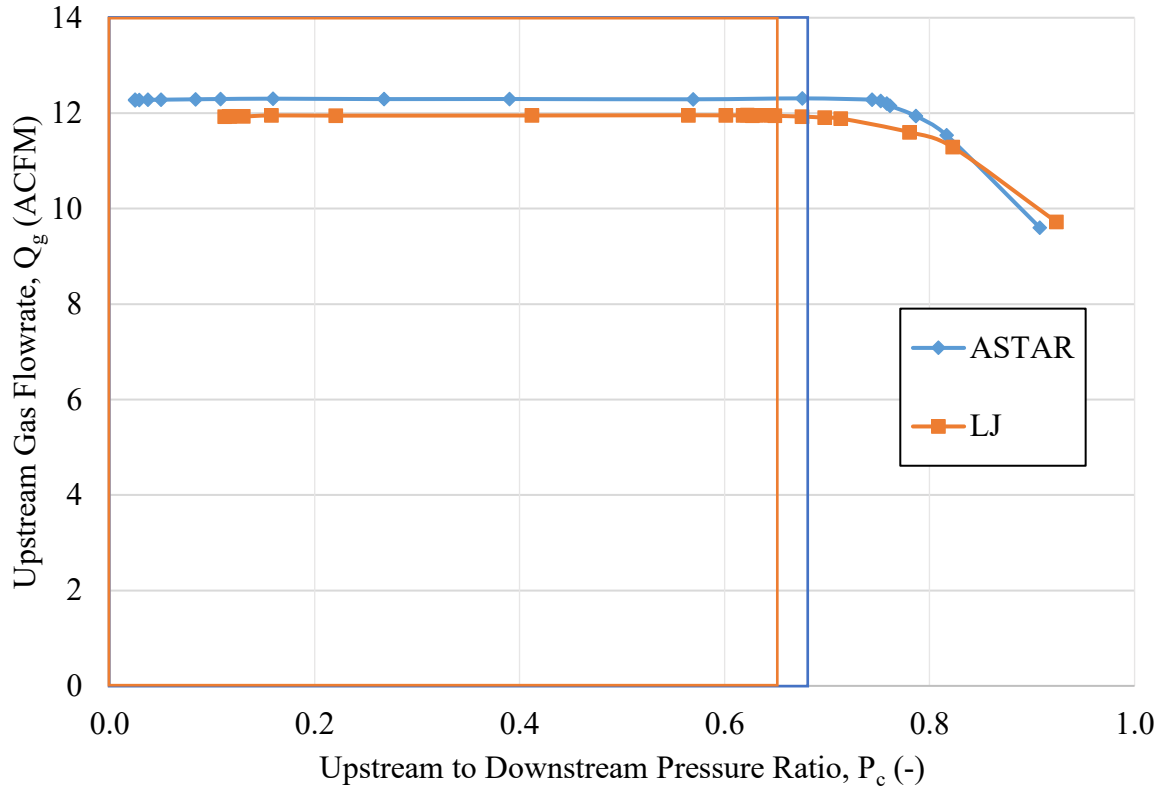


Figure 4.10 Effect of nozzle length on nozzle performance

Presence of pressure transducers along the nozzle body has an effect on the nozzle performance. As the fluid moves through the nozzle, the transducers make the flow more turbulent and this results in a higher pressure drop across the nozzle and hence a lower critical pressure ratio. In order to determine the effect of this turbulence, three nozzles were tested without the presence of pressure transducers on them. The results shown demonstrate the extent of impact of PTs on nozzle performance (Table 4.7). The critical pressure ratio on average lowered by 0.06 and the pressure drop across the nozzle increased by 2.5 psi due to the presence of pressure transducers. The effect of presence of PTs was more significant in some nozzles than others. This could be because the ends of PTs may have not been aligned with the inside surface of the nozzle to the same length each time.

Table 4.7 Effect of Pressure Transducers on Nozzle Performance

Nozzle	PTs installed on nozzle			No PTs installed on nozzle		
	ASTAR N1	Convex Bell N1	Deich N1	ASTAR N1	Convex Bell N1	Deich N1
<b>Critical Pressure Ratio</b>	0.75	0.41	0.53	0.81	0.42	0.61
<b>Pressure Drop</b>	6.0	15.1	12.3	4.1	13.9	7.8

### 4.3 Modelling – Single Phase Horizontal Flow

An empirical model was created based on data obtained from experiments and the geometrical parameters of the nozzle to determine the effect of surface areas of convergent and divergent sections on nozzle performance. Dimensionless analysis was performed to model the change in surface area along the nozzle. Such analysis was chosen to determine the critical pressure ratio of certain nozzle groups given the experimental conditions are similar to those in this experiment. The dimensionless number created for this purpose,

$$X = \frac{\text{Convergent Section Surface Area}}{\text{Throat Section Surface Area} + \text{Divergent Section Surface Area}} \quad (4.1)$$

$$X = \frac{S_{con}}{S_{th} + S_{div}} \quad (4.2)$$

To calculate the surface area for different sections of a nozzle, the equations used to create nozzle profile were used. The changing surface area through different regions of the nozzle was calculated by the following integral:

$$\text{Area} = \int_{x_1}^{x_2} y(x)dx \quad (4.3)$$

The area of seven basic regions had to be evaluated in order to account for all nozzles within one equation – three convergent regions, one throat region and three divergent regions. Three convergent regions include linear section, circular section and concave circular transition

section. Nozzle groups with converging linear section include – Rao Bell, Modified Rao Bell, Convex, Conical group 1 and Conical group 2 and LJ. Nozzles with converging concave circular section include – ASTAR, LJ and Moby Dick. Nozzles with converging circular transition section include - Rao Bell, Modified Rao Bell, Concave, Convex, ASTAR, LJ, Moby Dick and Deich. The throat region surface area was calculated for Modified Rao Bell, Convex, Concave, Moby Dick, Deich and Conical group 2. Three different divergent sections include concave circular section, parabolic section and linear section. Nozzles with diverging concave circular section include - Rao Bell, Modified Rao Bell, Concave, ASTAR, LJ and Deich. Nozzles with diverging parabolic section include - Rao Bell, Modified Rao Bell, Concave, Convex, ASTAR, LJ and Deich. Nozzles with diverging linear section include - Conical group 1, Conical group 2, LJ and Moby Dick.

Equation representing converging linear section is given as:

$$S_{lin,c} = 2\pi \int_{L_c}^{\pm \cos(\alpha_1-180)m_1R_t} [\tan(\alpha_1 - 180) x + \sin(\alpha_1 \pm 180) m_1R_t + m_1R_t + R_t - (\tan^{-1}(\alpha_1 - 180) \pm \cos(\alpha_1 - 180) m_1R_t) ] dx \quad (4.4)$$

Equation representing converging circular section is given as:

$$S_{cir,c} = 2\pi \int_{L_c}^{\pm \cos(\alpha_1-180)m_1R_t} [a_0x^2 + b_0x + c_0 ] dx \quad (4.5)$$

Equation representing converging concave circular transition section is given as:

$$S_{ct,c} = 2\pi \int_{\pm \cos(\alpha_1-180)m_1R_t}^{\pm \cos(\alpha_2-180)m_1R_t} [a_1x^2 + b_1x + c_1 ] dx \quad (4.6)$$

Equation representing throat section is given as:

$$S_{th} = 2\pi \int_{\cos(\alpha_2-180)m_1R_t}^{L_t} [R_t x] dx \quad (4.7)$$

Equation representing diverging concave circular transition section is given as:

$$S_{ct,d} = 2\pi \int_{L_t}^{\cos(\beta_2-90)m_2R_t+L_t} [a_2x^2 + b_2x + c_2] dx \quad (4.8)$$

Equation representing diverging parabolic section is given as:

$$S_{p,d} = 2\pi \int_{\cos(\beta_2-90)m_2R_t+L_t}^{L_d+L_t} [A_px^2 + B_px + C_p] dx \quad (4.9)$$

Equation representing diverging linear section is given as:

$$S_{lin,d} = 2\pi \int_{\cos(\beta_2-90)m_2R_t+L_t}^{L_d+L_t} [\tan(\beta_2)x + \sin(\beta_1 - 180) m_2R_t + m_2R_t + R_t - (\tan(\beta_2 - 180) m_2R_t)] dx \quad (4.10)$$

Substituting Equations 4.4 – 4.10 in Equation 2,

$$X = \frac{S_{linear,c} + S_{cir,c} + S_{ct,c}}{S_{th} + S_{ct,d} + S_{p,d} + S_{linear,d}} \quad (4.11)$$

Since not all nozzle geometries include all terms in Equation 4.11, each term in this equation was multiplied by a Kronecker delta. So, if that particular section exists as part of the nozzle geometry then the delta value is 1, else it is 0. Applying this, Equation 4.11 modifies to

$$X = \frac{\delta_1 S_{lin,c} + \delta_2 S_{cir,c} + \delta_3 S_{ct,c}}{\delta_4 S_{th} + \delta_5 S_{ct,d} + \delta_6 S_{p,d} + \delta_7 S_{lin,d}} \quad (4.12)$$

Equation 4.12 was used to calculate ‘X’ values for all nozzles tested. Value of ‘X’ for corresponding nozzles is shown in Table 4.8. Figure 4.11 (Pg. 65) shows a plot where ‘X’ is plotted against the critical pressure ratio of each nozzle.

Table 4.8 Calculated Values of Dimensionless Number for Nozzle Tested

Nozzle			Dimensionless Number, X (-)
Conical	Group 1	Nozzle 2	0.14
		Nozzle 3	0.10
		Nozzle 4	0.24
	Group 2	Nozzle 1	0.14
		Nozzle 3	0.12
Parabolic	Rao Bell	Nozzle 1	0.32
		Nozzle 3	0.29
		Nozzle 4	0.28
		Nozzle 5	0.30
	Modified Rao Bell	Nozzle 3	0.30
		Nozzle 7	0.27
		Nozzle 8	0.24
	Convex Bell	Nozzle 1	1.58
	Concave Bell	Nozzle 1	0.44
		Nozzle 2	0.41
	ASTAR	Nozzle 1	1.63
		Nozzle 2	0.93
		Nozzle 3	0.60
	Moby Dick	Nozzle 1	4.18
		Nozzle 2	2.86
		Nozzle 4	0.82
Deich	Nozzle 1	1.17	
	Nozzle 2	1.06	
	Nozzle 3	0.82	
LJ	Nozzle 1	0.15	

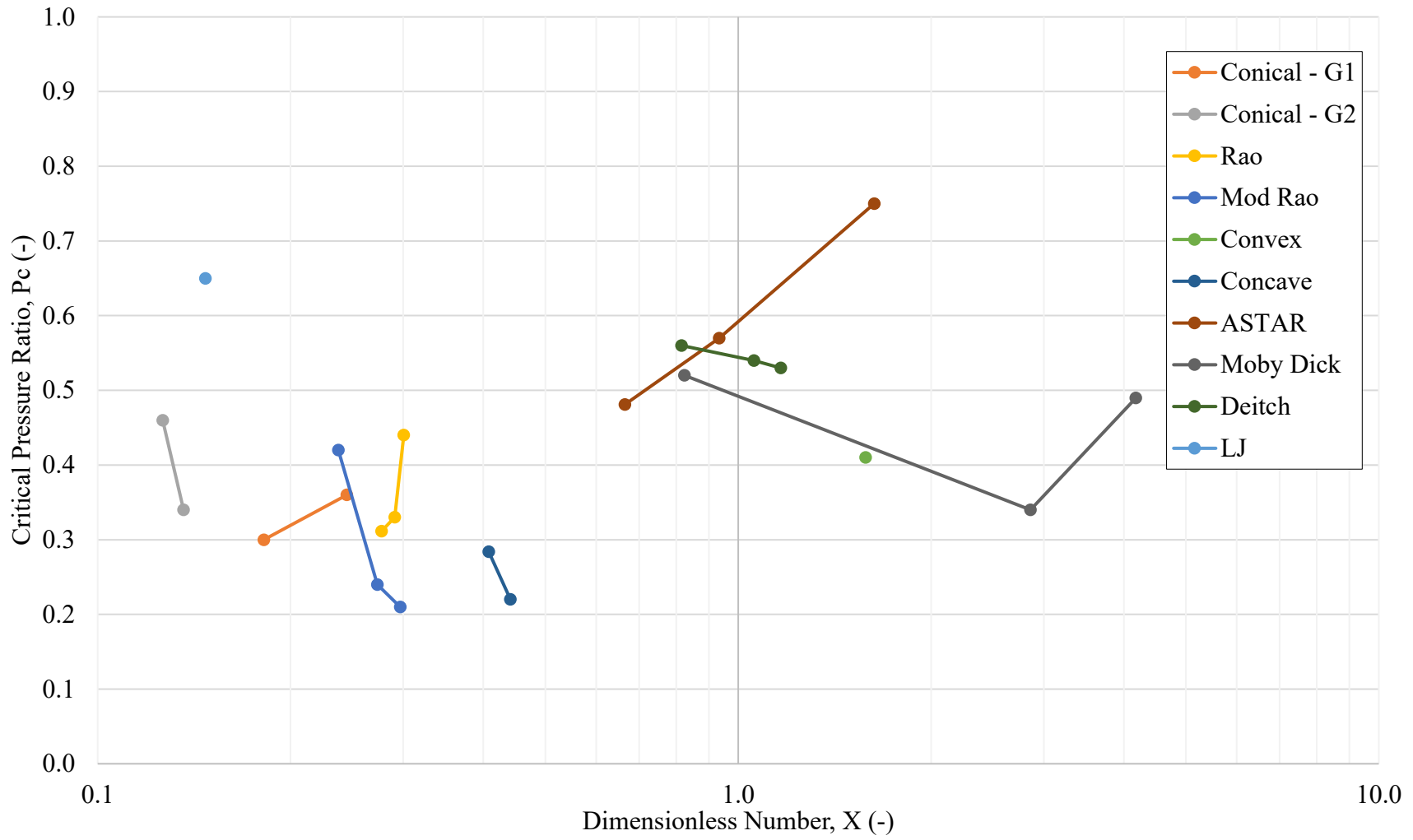


Figure 4.11 Effect of converging, throat and diverging surface area on nozzle configuration performance by applying dimensionless analysis

If an ideal critical pressure ratio of 0.6 was arbitrarily selected and were to introduce pressure drop across the nozzle as part of the plot, shown in Figure 4.12, those nozzle where the critical pressure ratio is above the blue line and the pressure drop value is below the green line (pressure drop of 15 psi) would be considered ideal. It can be observed that generally those nozzles with dimensionless number  $0.6 < X < 2$  or  $X$  close to 1 performed well, with an outlier of LJ nozzle. Therefore, generally those nozzles where the area of convergent section is close in value to the sum of the area of divergent section and throat section performed well in single phase gas testing.

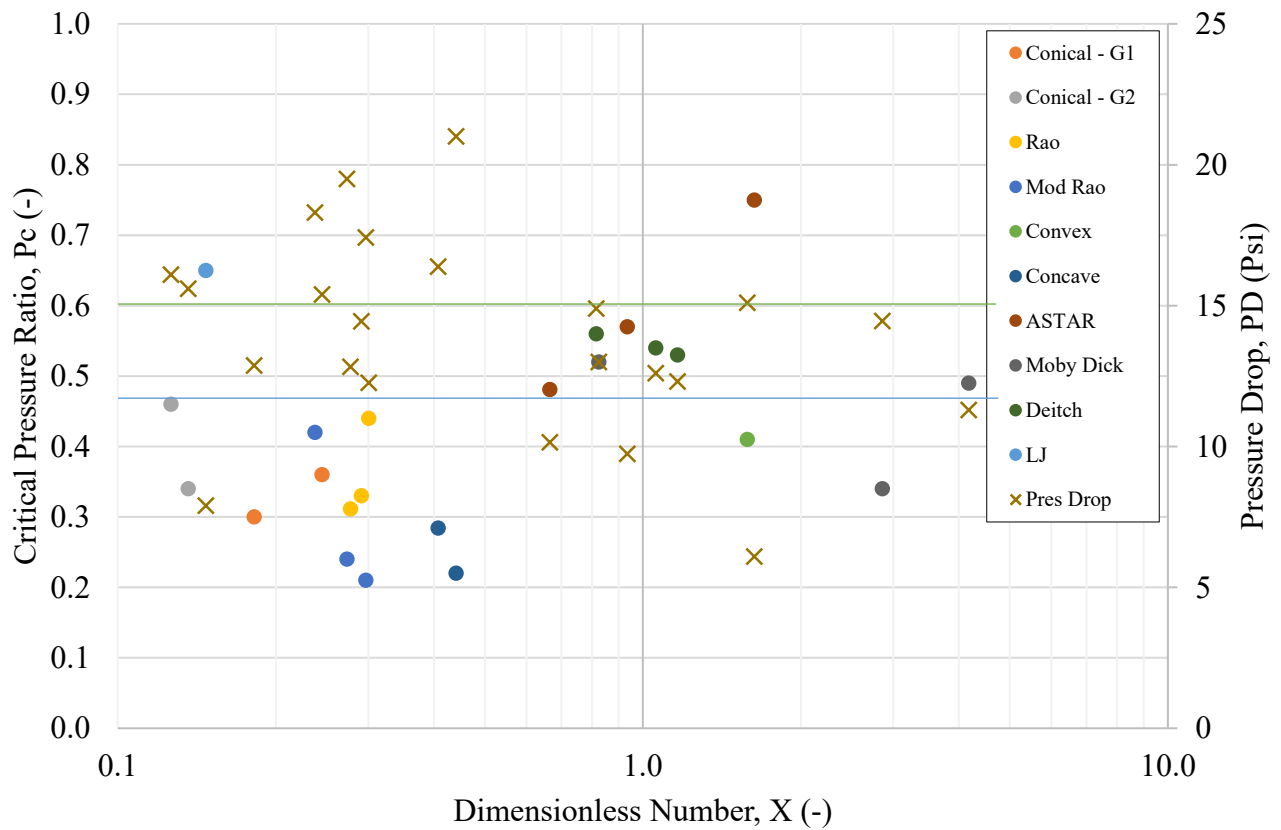


Figure 4.12 Pressure drop and critical pressure ratio against X to determine the optimal geometries

Using this model, trends regarding change in diverging angles for basic conical and parabolic shapes and trends regarding presence of an elongated throat can be obtained. Figure 4.13 shows the effect on performance of nozzle if the throat length is not changed, but only the diverging angle is changed. Nozzles with a smaller diverging angle have a higher value of 'X'. And it can be noted from Figure 4.13 that as X increases for a particular geometry group, the nozzle with a smaller diverging angle has a higher critical pressure ratio. Figure 4.14 shows the effect on performance of nozzle if the diverging angle is kept constant and the throat is elongated. An increasing throat length, results in a lower 'X' value. And from the plot it can be noted that as X decreases for a particular geometry group, the nozzle with a higher throat length resulted in a higher critical pressure ratio.

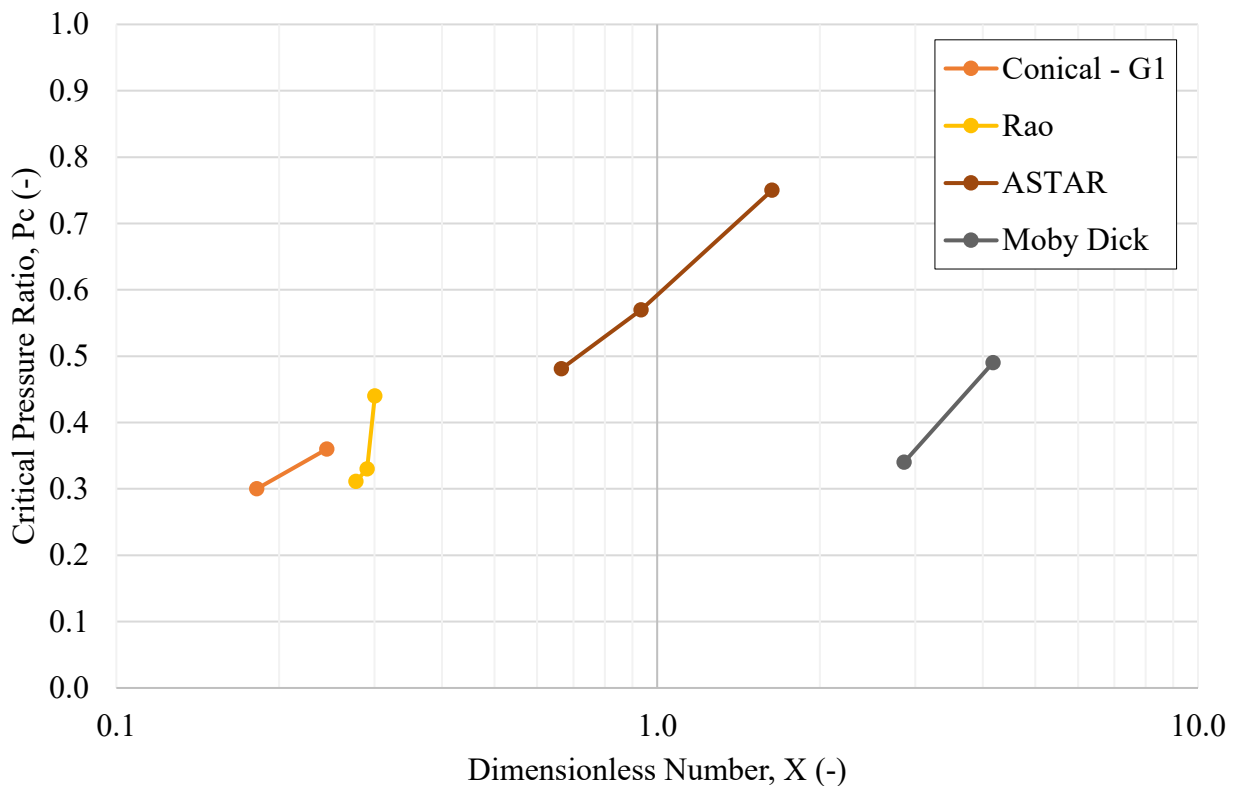


Figure 4.13 Effect on nozzle performance of varying diverging angle for different nozzle geometry groups

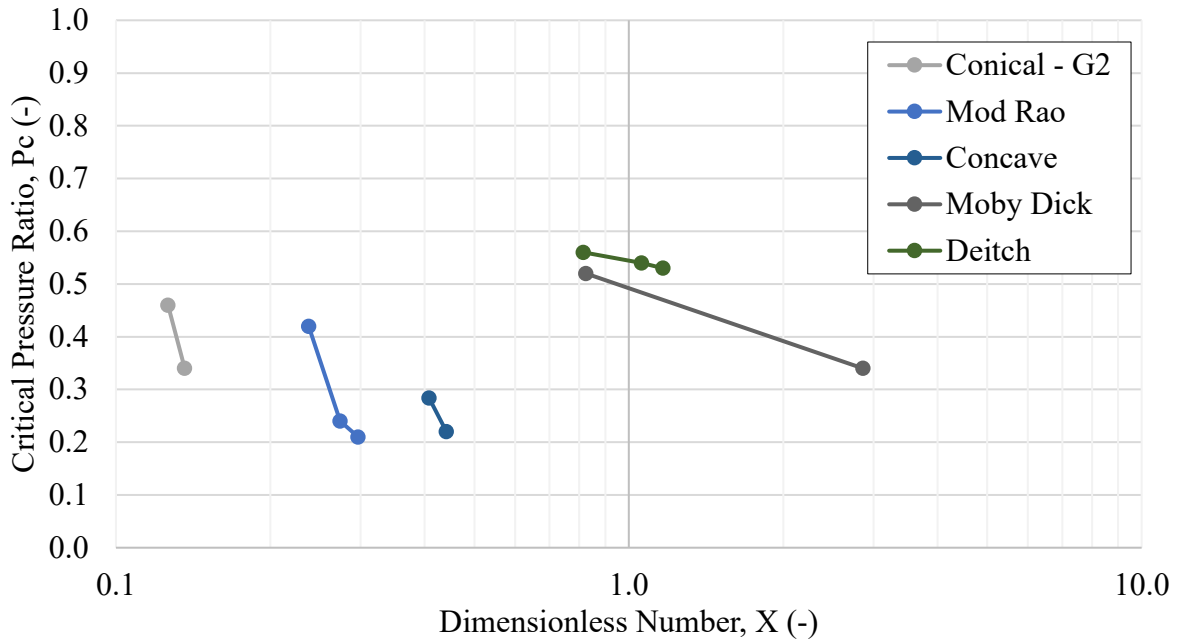


Figure 4.14 Effect on nozzle performance of varying throat length for different nozzle geometry groups

#### 4.4 Data Analysis – Two-Phase Horizontal Flow

Similar analysis as for single-phase horizontal flow was performed to two-phase horizontal flow experiments to determine the most optimum nozzle geometry. The six nozzles tested were ranked separately based on the critical pressure ratios, as shown in Table 4.9, and based on the pressure drop, as shown in Table 4.10. Then in Table 4.11, the two best geometries were determined (highlighted in red) based on the nozzle geometry that performed well in both cases. The ASTAR nozzle geometries performed well in both criteria. However, the two phase horizontal flow rankings were different from single phase horizontal flow rankings, probably a result of higher upstream pressure, lower gas flowrate and turbulence due to the presence of liquid phase. Also, the critical pressure ratio value of conical group 1 nozzle 4 behaved opposite of what was expected – critical pressure ratio value is supposed to lower when a second phase is introduced. This could be a result of different upstream conditions in two-phase tests.

Table 4.9 Ranking of Nozzle Performance Based on Critical Pressure Ratio

Rank	Nozzle Name	Critical Pressure Ratio, Pc (-)
1	ASTAR - Nozzle 2	0.55
2	ASTAR - Nozzle 1	0.50
3	Conical Group 1 - Nozzle 4	0.45
4	Moby Dick - Nozzle 1	0.43
5	Deich - Nozzle 1	0.42
6	LJ – Nozzle 1	0.36

Table 4.10 Ranking of Nozzle Performance Based on Pressure Drop Across the Nozzle

Rank	Nozzle Name	Pressure Drop, PD (psi)
1	ASTAR - Nozzle 2	16.4
2	Conical Group 1 - Nozzle 4	18.5
3	ASTAR - Nozzle 1	21.0
4	Moby Dick - Nozzle 1	22.0
5	LJ – Nozzle 1	25.0
6	Deich - Nozzle 1	27.5

Table 4.11 Rank of Nozzle Performance Based on Both Critical Pressure Ratio and Pressure Drop

Nozzle Name	Critical Pressure Ratio, Pc (-)	Pressure Drop, PD (psi)
ASTAR - Nozzle 2	1	1
ASTAR - Nozzle 1	2	3
Conical Group 1 - Nozzle 4	3	2
Moby Dick - Nozzle 1	4	4
Deich - Nozzle 1	5	6
LJ – Nozzle 1	6	5

In order to conduct pressure drop analysis along the nozzle, similar procedure as for single-phase horizontal tests was used, except the nozzle body was divided into three regions instead of four – pipe to the convergent section, convergent section to throat to divergent section and divergent section to the pipe area. Based on this, Figure 4.15 was plotted. It can be noted that pressure recovery is highest for the ASTAR nozzles followed by the Conical nozzle. Pressure recovery was seen in all the nozzles that were tested, unlike single phase where there was minimum pressure recovery among non-optimal geometries.

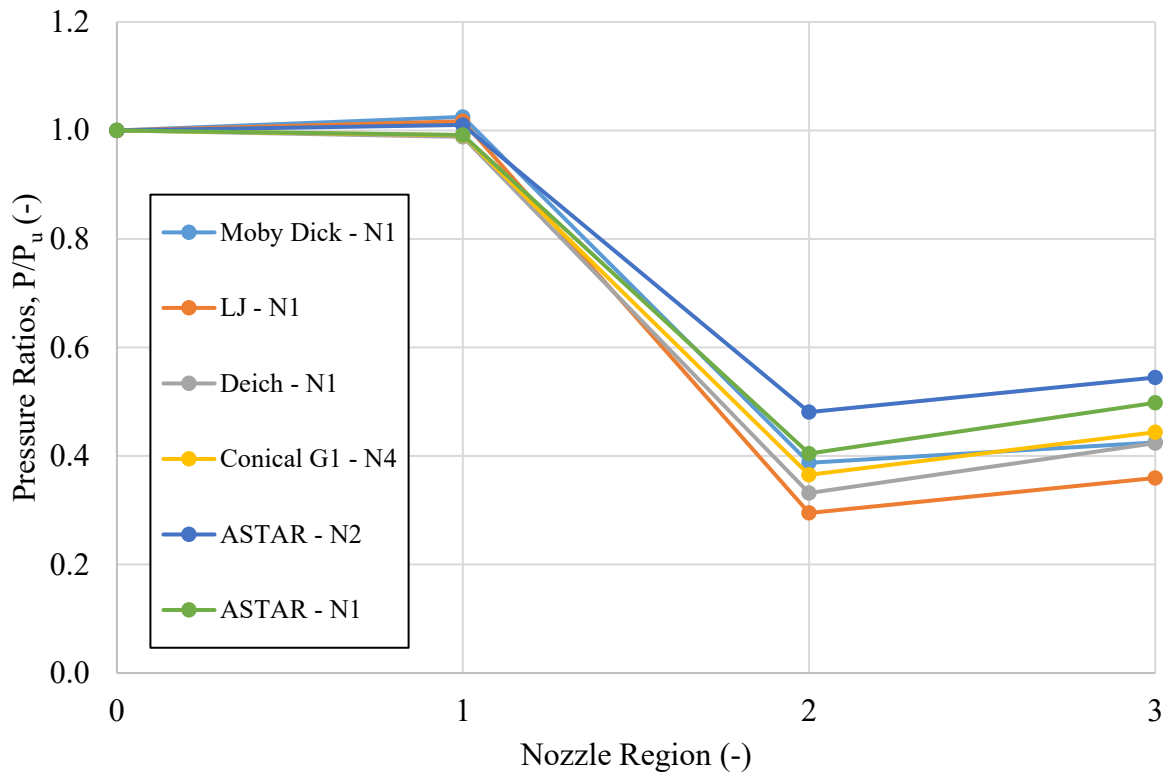


Figure 4.15 Pressure drop ratio across nozzle for two-phase horizontal flow tests

Since two phases were used in these experiments, analysis of flow pattern upstream and downstream the nozzle provided some information regarding the nozzle performance. For all experiments, the flow upstream the nozzle was kept stratified at all times (Figure 4.16). The

flow at the exit of the nozzle resembled an annular churn flow pattern (Figure 4.17) before turning back to stratified flow. The length of annular churn flow pattern downstream the nozzle when there was no back pressure on the flow (back pressure valve open 100%) was recorded. Figure 4.18 shows the results of different nozzle critical pressure ratios when plotted against the downstream distance. The trendline of this plot shows a decreasing trend, i.e., as the length of turbulent churn flow pattern downstream of a nozzle decreased, the nozzle performed better in terms of critical pressure ratio.



Figure 4.16 Stratified flow pattern upstream of nozzle



Figure 4.17 Annular churn flow pattern downstream of nozzle before turning back to stratified flow

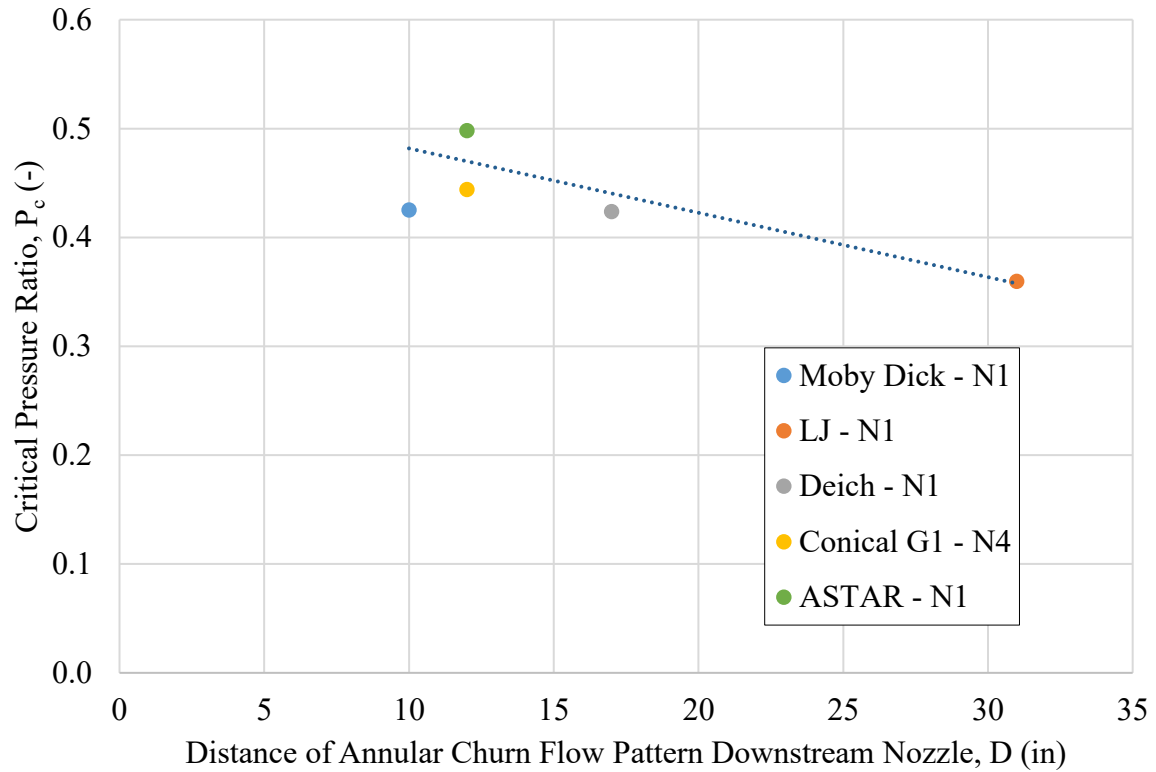


Figure 4.18 Effect of length of annular churn flow pattern downstream of nozzle on nozzle performance

#### 4.5 Data Analysis – Two-Phase Vertical Flow

For this set of experiments, same six nozzle geometries as phase 2 were tested in a two-phase vertical flow loop. From the results it can be noted that the ASTAR nozzle geometries perform better than other nozzle geometry groups. In both criteria of critical pressure ratio and pressure drop across the nozzle, these geometries perform the best. And, ASTAR nozzle 2 geometry in particular outperforms ASTAR nozzle 1 geometry in both criteria.

Comparing these results to results obtained from two-phase horizontal testing, it can be noted that the LJ nozzle did not perform as expected. In general, the critical pressure ratio is supposed to be a lower value for vertical testing compared to horizontal testing. But, opposite of this was observed in case of LJ nozzle. Critical pressure ratio was higher by 0.05. This could be a

result of varying upstream conditions during horizontal and vertical experiments. For all the other nozzles, there was drop noticed in the value of critical pressure ratio and an increase in pressure drop across the nozzle, as expected due to gravitational pressure losses.

From the data obtained, it can also be noted that there is a drop in the temperature downstream of nozzle. As the fluid flows out of the nozzle, the gas expands and the frequency of collisions between the gas particles decreases. Because of this, less heat is generated and the fluid cools as it expands. This can be observed in data obtained for all the nozzles, there is an average drop of 6 °F. The drop in temperature downstream the nozzle varies for different nozzles at the point of their respective critical pressure ratios. This may have a possible link to how much does the gas expand once it comes out of each nozzle.

In horizontal flow, the temperature after the nozzle increases but in case of vertical flow the temperature of fluid downstream the nozzle is lower than the temperature of fluid upstream nozzle (Table 4.12). Similar temperature behavior is not noticed in horizontal flow as in vertical flow because of the point at which the temperature reading was taken for horizontal flow tests. The downstream temperature was recorded after the flow pattern has changed back to stratified. This means that the gas is no longer expanding, but is compressing which increased the temperature observed.

Comparing these results to single-phase horizontal flow results, it can be observed that the basic rankings of these nozzles did not change. ASTAR still performed best in both cases, followed by LJ nozzle, Deich nozzle, Moby Dick nozzle and Conical group 1 nozzle 4. This demonstrates that if there is a need to evaluate the nozzles strictly on the basis of critical pressure ratios and pressure drops across the nozzle, single phase testing horizontal tested can be done, which is a much easier set-up.

Table 4.12 Comparison of Data between Horizontal and Vertical Two Phase Flow

<b>Two Phase Flow</b>	<b>Vertical</b>	<b>Horizontal</b>
<b>Nozzle</b>	<b>ASTAR - Nozzle 1</b>	
<b>Critical Pressure Ratio, <math>P_c</math></b>	0.45	0.50
<b>Pressure Drop, <math>dP</math> (psi)</b>	24.8	21.0
<b>Upstream Pressure, <math>P_u</math> (psig)</b>	44.8	40.0
<b>Upstream Temperature, <math>T_u</math> (°F)</b>	130	66
<b>Downstream Temperature, <math>T_d</math> (°F)</b>	125	90
<b>Upstream Water Flowrate, <math>Q_{u,w}</math> (GPM)</b>	1.04	0.67
<b>Upstream Gas Flowrate, <math>Q_{u,g}</math> (ACFM)</b>	3.7	8.0

#### 4.5.1 Downstream Water Flowrate Analysis

For two-phase vertical experiments, downstream water flowrate was measured and evaluated. Water was flown into the second tank and the time it took for the tank to fill up with 4 lbs of water was measured. By considering water density as  $8.33 \text{ lb/ft}^3$ , volume of water filled was calculated. Finally the water flowrate was calculated by dividing the volume by time taken to fill the tank. Such measurements were repeated multiple times for the same backpressure valve opening percentage value. Below, in Table 4.13, the values obtained during testing of LJ nozzle when backpressure valve was open 5% is shown. From the data it can be observed that the water flowrate is a lower value after the back pressure valve percentage is changed (7.5 BPD) and then increases to 9.8 BPD. As time progress, the downstream flowrate stabilizes to a value of 8.3 BPD. This shows that the initial increase in downstream water flowrate is only a short-lived effect and transient behavior can be observed over time as the flowrate stabilizes.

Table 4.13 Downstream Water Flowrate Calculation Data and Results

Measurement no.	Back Pressure Valve Opening (%)	Average Pressure Ratio, $P_d/P_u$ (-)	Time, t (min)	Weight of Water, W (lbs)	Downstream Water Flowrate, $Q_w$ (BPD)
1	5	0.94	2.18	4	7.5
2			1.68		9.8
3			1.72		9.6
4			1.85		8.9
5			1.85		8.9
6			1.92		8.6
7			1.98		8.3
8			1.97		8.3
1	50	0.07	0.13	4	122.3
2			1.07		15.4
3			1.23		13.3
4			1.20		13.7
5			1.18		13.9
6			1.18		13.9
7			1.27		13.0
8			1.02		16.1
9			1.15		14.3
10			1.12		14.7
11			1.13		14.5
12			1.12		14.7
13			1.12		14.7
14			1.08		15.1
15			1.15		14.3
16			1.10		14.9
17			1.12		14.7
18			1.10		14.9
19			1.10		14.9
20			1.15		14.3
21			1.10		14.9

In order to simulate the effect of liquid loading in a gas well, the downstream to upstream pressure ratio was 0.94 (backpressure valve open 5%). Since the pressure differential between upstream and downstream of nozzle was low, there was a lot more accumulation. Next, the pressure ratio was changed to 0.07 (a larger pressure differential between upstream and downstream of nozzle) by opening the backpressure valve to a higher percentage (50%). This simulated the effect of unloading the well after liquid accumulation has occurred. It can be noted that the downstream water flowrate value immediately after the valve is opened to 50% is almost 15 times more than what it was when the valve was open 5%. This demonstrates that liquid that had accumulated in the tubing has now mobilized to top of the well due to an increase in gas flowrate, a result of increase in pressure differential. The transient behavior observed when valve was open 5% was also observed in this case. The downstream water flowrate eventually drops to about 14.8 BPD.

## CHAPTER 5

### CONCLUSIONS AND RECOMMENDATIONS

Two-phase and single-phase flow experiments were successfully performed to determine the optimal nozzle geometry that can be implemented to mitigate the impact of liquid loading. Single-phase horizontal flow experimental results were analyzed to determine the effect nozzle parameters had on nozzle performance and an empirical model was developed to predict the critical pressure ratio based on the area of the nozzle at given conditions. Two-phase horizontal flow experimental results helped to determine the effect of introducing water into the system. Two-phase vertical tests helped determine the optimal nozzle geometry that can be used to deliquesfy gas wells.

#### 5.1 Conclusions

Based on analysis of data obtained from all three phases, the following conclusions can be drawn from this research study:

- Nozzle geometry does have a significant impact of nozzle performance. Effect of single-phase air flow through a nozzle revealed the effect of different nozzle parameters on nozzle performance. A lower diverging angle and no elongated throat gave the best critical pressure ratio and a low pressure drop. The length of the nozzle did not have as much of an effect on the performance as the shape of the nozzle right before and after the throat. And the shape of diverging section is important to promote pressure recovery.
- An empirical model was developed for single-phase flow to predict the effect of surface area on nozzle performance and determine the critical pressure ratio by calculating the dimensionless number 'X'.

- Two-phase flow resulted in a lower critical pressure ratio and a higher pressure drop across the nozzle due to pressure losses caused by turbulence with the presence of liquid. It was also determined that the distance of annular churn flow pattern downstream the nozzle may have an impact of nozzle performance.
- Similar trends related to critical pressure ratio and pressure drop across the nozzle were observed between single-phase horizontal flow tests and two-phase vertical flow tests. Therefore, to determine how a geometry is going to perform based on the two above-mentioned criteria, single-phase testing is a better option. This is because single-phase testing is easier to conduct and is also a less expensive option.
- From two-phase vertical experiments, ASTAR nozzle 2 geometry was chosen as the most optimal geometry to deliquefy gas wells after single-phase and two-phase experimental tests. This geometry has a diverging angle of  $10^\circ$ , a parabolic diverging section, no elongated throat and a convex and concave converging section. This geometry performed best in both criteria on which the nozzles were ranked.

## **5.2 Future Work Recommendation**

For future work, more nozzle geometries can be tested in the existing two-phase vertical facility to gather data in order to further evaluate the efficiency of nozzle geometries to deliquefy gas wells. The existing facility can also be modified for different pipe diameters and GLR to note the effect of these parameters on nozzle performance. From these tests a more comprehensive mechanistic model can be developed to model flow two-phase flow through nozzle. This model can be similar to the existing model for chokes, but one that account for the diffuser section and the slip condition between liquid and gas phase. The experimental results obtained can be

modelled using CFD simulations to develop accurate simulations for two-phase flow through nozzle.

## REFERENCES

- Arellano, J.L., Ermel, E., 2015. Systeem, Apparatus and Method for Well Deliquification. United States Patent Application Publication, US20150053410A1.
- Ashford, F.E., Pierce, P.E., 1975. Determining Multiphase Pressure Drops and Flow Capacities in Down-Hole Safety Valves. *J. Pet. Technol.* 27, 1145–1152. <https://doi.org/10.2118/5161-PA>
- Ashwood, P.F., Higgins, D.G., 1957. The Influence of Design Pressure Ratio and Divergence Angle on the Thrust of Convergent-Divergent Propelling Nozzles. *Aeronautical Research Council. C.P. No. 325*
- Barber, R.E., Schultheiss, M.J., 1967. Effect of Nozzle Geometry on Off-Design Performance of Partial Admission Impulse Turbines. Office of Naval Research, 49-52. PR010-04-01
- Bestion, D., 1990. The physical closure laws in the CATHARE code. *Nucl. Eng. Des.* 124, 229–245. [https://doi.org/10.1016/0029-5493\(90\)90294-8](https://doi.org/10.1016/0029-5493(90)90294-8)
- Chang, P., Bai, B., 2017. An improved method of gas well deliquification using supersonic nozzle. *Int. J. Heat Mass Transf.* 108, 2262–2272. <https://doi.org/10.1016/j.ijheatmasstransfer.2017.01.054>
- Clarke, C.J., Carswell, B., 2007. Principles of astrophysical fluid dynamics. Cambridge, UK: Cambridge University Press.
- EIA, 2018. Number of Producing Gas Wells (29 September 2017 revision). [https://www.eia.gov/dnav/ng/ng\\_prod\\_wells\\_sl\\_a.htm](https://www.eia.gov/dnav/ng/ng_prod_wells_sl_a.htm) (accessed 18 October 2017).
- Elliot, D.G., Weinber, E., 1968. Acceleration of Liquids in Two-Phase Nozzles. 16-34. Jet Propulsion Lab, Pasadena, CA. <https://doi.org/19680017730>
- Joseph, A., Sand, C.M., Ajiienka, J.A., 2013. Classification and Management of Liquid Loading in Gas Wells. Paper SPE 167603 presented at the SPE Nigeria Annual International Conference and Exhibition, Lagos, Nigeria, 5-7 August. <https://doi.org/10.2118/167603-MS>
- King, G.E., 2005. Low Pressure Gas Well Deliverability Issues: Common Loading Causes, Diagnostics and Effective Deliquidation Practices. *Brownfields: Optimizing Mature Assets Conference*, 19-20 September, Denver, Colorado.
- Kulhanek, S.L., 2012. Design, Analysis, and Simulation of Rocket Propulsion System. MS Thesis, University of Kansas, Lawrence, Kansas. (June 2012)
- Lea, J.F., Nickens, H. V., 2004. Solving Gas-Well Liquid-Loading Problems. *J. Pet. Technol.* 56, 30–36. <https://doi.org/10.2118/72092-JPT>

- Levitan, L.L., Salygin, V.V, Yurchenko, V.D., 2000. Method and Apparatus for Withdrawal of Liquid Phase from Wellbores. Unites States Patent Application Publication, US006059040A.
- Mason, K., Scheinder, G., 2007. Venturi Siphon Atomization Liquid Lift Apparatus and Method. Unites States Patent Application Publication, US20070221383A1.
- Nair, J., Pereyra, E., Sarica, C., Torres, C.F., Arellano, J.M., 2015. Downhole Venturi Nozzles and Foam Application: A Novel Artificial Lift Method. Paper SPE 173630 presented at SPE Production and Operations Symposium, 1-5 March, Oklahoma City, Oklahoma. <https://doi.org/10.2118/173630-MS>
- Nürnberg-Genin, C., Stark, R., 2009. Flow transition in dual bell nozzles. *Shock Waves* 19, 265–270. <https://doi.org/10.1007/s00193-008-0176-4>
- Östlund, J., 2002. Flow Processes in Rocket Engine Nozzles with Focus on Flow Separation and Side-loads. Royal Institute of Technology. <https://doi.org/0348467X>
- Oudeman, P., 2007. On the Flow Performance of Velocity Strings to Unload Wet Gas Wells. Paper 104605 presented at SPE Middle East Oil and Gas Show and Conference, 11-14 March, Kingdom of Bahrain. <https://doi.org/10.2523/104605-MS>
- Popov, S.A., 2002. Liquid-Gas Ejector with an Improved Liquid Nozzle and Variants. United States Patent Application Publication, US20020079384A1.
- Rahman, A., Amin, A., Hossain, A., Fleck, B., 2014. Numerical investigation of two-phase nozzle flow. *Procedia Eng.* 90, 346–350. <https://doi.org/10.1016/j.proeng.2014.11.860>
- Raiano M., 2013. Rocket Engines, 21 November 2013, <http://www.aerospacengineering.net/?p=1241> (accessed 7 March 2018)
- Staedtke, H., Franchello, G., Worth, B. et al., 2005. Advanced Three-Dimensional Two-Phase Flow Simulation Tools for Application to Reactor Safety (ASTAR). *Nucl. Eng. Des.* 235, 379–400. <https://doi.org/10.1016/j.nucengdes.2004.08.052>
- Sutton, G., Biblarz, O., 2001. *Rocket Propulsion Elements, Rocket propulsion elements.* Wiley. <https://doi.org/10.1017/CBO9781107415324.004>
- Turner, R.G., Hubbard, M.G., Dukler, A.E., 1969. Analysis and Prediction of Minimum Flow Rate for the Continuous Removal of Liquids from Gas Wells. *J. Pet. Technol.* 21, 1475–1482. <https://doi.org/10.2118/2198-PA>
- Xue, J., Jog, M. A., Jeng, S.M. et al., 2002. Influence of Geometry on the Performance of Simplex Nozzles under Constant Pressure Drop, ILASS Americas. 15<sup>th</sup> Annual conference on Liquid Atomization and Spray Systems, May 2002, Madison, Wisconsin.